Exotic superconducting circuits to probe and protect quantum states of light and matter

Zaki Leghtas

Research Direction Habilitation from ENS Paris

Exotic superconducting circuits to probe and protect quantum states of light and matter

Zaki LEGHTAS

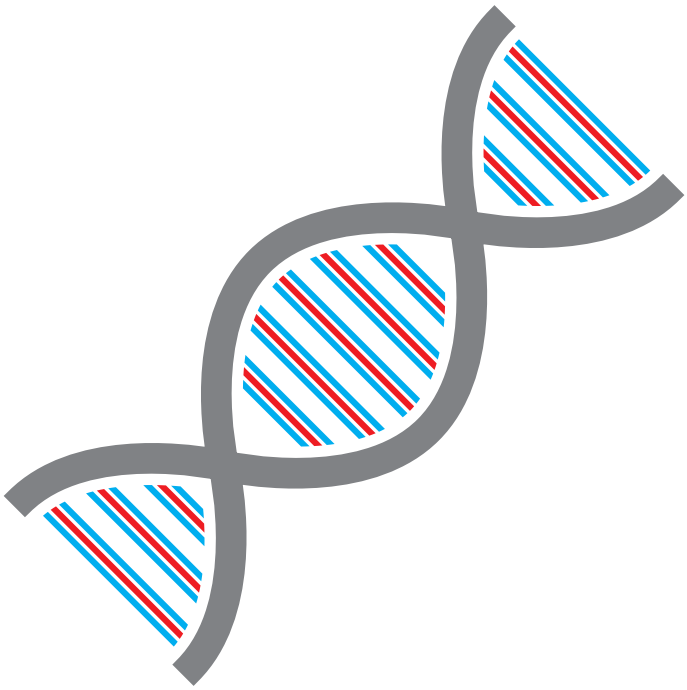

Defended on November 6th 2020

Members of the jury

Çağlar Girit ..... Rapporteur

Hugues Pothier ..... Rapporteur

Peter Zoller ..... Rapporteur

Takis Kontos ..... Examinateur

Jean-Michel Raimond ..... Examinateur

Remerciements

Je souhaiterais commencer par remercier les membres du jury: Peter Zoller, Hugues Pothier, Caglar Girit, Jean-Michel Raimond et Takis Kontos, pour avoir lu ce manuscrit avec autant d'attention et d'avoir préparé une série de questions redoutables.

Merci à Pierre Rouchon, Mazyar Mirrahimi et Alain Sarlette, qui incarnent pour moi le noyau dur de ma famille scientifique. Au fil des années, les excursions des uns et des autres ont élargi nos connaissances, aiguisé nos outils et affiné notre vision. Je me réjouis de poursuivre cette construction à leurs côtés. Merci à Philippe Campagne-Ibarcq de nous avoir rejoint récemment en apportant un nouveau souffle et sa propre curiosité qui irrigue l'équipe de nouvelles idées.

Merci à tous les membres de l'équipe Hardware Quantic: Clarke Smith, Marius Villiers, Camille Berdou, Aron Vanselow, Ulysse Rélgade et Alvise Borgognoni. Construire des expériences avec vous me passionne tous les jours.

Merci à toute l'équipe HQC, et en particulier Matthieu Delbecq, Audrey Cottet, William Legrand et enfin Takis Kontos pour l'énergie immense qu'il déploie pour que nous travaillions dans les meilleurs conditions possibles, et pour la générosité avec laquelle il partage ses profondes connaissances scientifiques.

Merci à Emmanuel Flurin pour sa créativité sans limite. Merci à Samuel Deléglise de nous avoir présenté les résonnateurs mécaniques permettant d'ouvrir de nouvelles perspectives passionantes aux circuits quantiques.

Merci à Alice & Bob: Raphaël Lescanne, Théau Peronnin, Sébastien Jezouin, Jérémie Guillaud et Anil Murani, pour votre ambition démeusurée et votre travail acharné qui m'inspirent.

Merci à Benjamin Huard de m'avoir acceuilli à l'ENS à mon arrivée à Paris, de m'avoir soutenu pour monter ma propre activité expérimentale après son départ et pour nos collaborations présentes et futurs.

Merci à Benoit Douçoit pour ces longues discussions fantastiques où je pose une question

floue et confuse, et au fil de ses explications l'image s'aiguise.

Merci à Caglar Girit et Jean-Loup Smirr de nous donner accès à leur salle blanche, sans quoi aucun de nos échantillons ne pourrait être fabriqué.

Merci à tous les membres du CAS et en particulier à Nicolas Petit pour sa gestion par la confiance.

Merci à José Palomo pour son engagement dans le développement de couches minces supraconductives.

Enfin, mille mercis au département de physique de l'ENS d'avoir crée un environnement scientifique à la fois convivial et rigoureux. Merci à la direction: Jean-Marc Berroir, Jean-Michel Isac, Laura Baron-Ledez, Anne Matignon, Christine Chambon, Valérie Diologent, Olga Hodges. Merci au service infrastructures: Didier Courtiade, Catherine Gripe, Théo Charpentier, Céline Da Silva, Dimitri Courtiade, Cyrille Le Gallo. Merci à la salle blanche: Michael Rosticher, Aurélie Pierret, José Palomo. Merci au service électronique: Philippe Pace, Anne Denis. Merci au service cryogénie: Olivier Andrieu, Florent Perrin. Merci au service mécanique: Nabil Garroum, Arnaud Leclercq, Pascal Morfin, Anaelle Pascal, Jules Silembo, Mathieu Sardin, Quentin Anty, Allan Hourdry, Aboubakar Lassana, Georges Cornudet, José Da-Silva-Quintas. Merci au service informatique: Christophe Bonnet, Yann Colin, Zaire Dissi. Merci au service électrique: Franck Bouchereau, Jean-Marc Jusseau, Philippe Rousseau.

Ce qui est douloureux, c'est qu'il est impossible d'expliquer quelque chose à quelqu'un qui ne l'a pas déjà compris. On peut seulement parler à quelqu'un qui en a le pressentiment et qui souffre de ne pas avoir de lumières là-dessus.

Christian Bobin

Contents

Chapter 1

Scientific profile

Personal information

Zaki Leghtas

ORCID: 0000-0002-9172-1537

Date of birth: 25/12/1986

Nationality: British

http://cas.ensmp.fr/~leghtas/

Education

• 2009 – 2012: PhD : Quantum state engineering and stabilization (theory)
Mines ParisTech / INRIA Paris
Supervisors : Pierre Rouchon and Mazyar Mirrahimi

• 2006 – 2009: Masters of science and engineering, Mines ParisTech, Paris

Current positions

• Dec 2015 – : Assiociate Professor at Mines ParisTech, Paris
Member of the Laboratoire de Physique de l'Ecole Normale Supérieure, Paris
Member of the QUANTIC team, INRIA, Paris

Previous position

• 2012 – 2015: Postdoctoral researcher in the group of Michel Devoret at Yale University.
Topic: Driven dissipative superconducting quantum circuits (experiments)

Grants

• 2020 - 2025 ERC starting grant 1500 k€

• 2020 - 2023 Quantera 300 k€

• 2018 - Sirteq 50 k€

• 2016 - 2019 EMERGENCE Ville de Paris 230 k€

• 2016 - 2020 ANR accueil chercheur haut niveau 400 k€

Supervision of graduate students and postdoctoral fellows

Postdocs: • Clarke Smith

Students: • Camille Berdou • Marius Villiers • Ulysse Réglade

Alumni: • Raphaël Lescanne • Lucas Verney

Teaching activities

• 2018 – : Quantum information – graduate (30h / year)

• 2016 – : Quantum and statistical physics – graduate (15h / year)

• 2016 – 2018: Quantum physics – undergraduate (30h / year)

Organization of scientific meetings

• Nov 2018 : Organizing committee for "International Conference on Quantum Computation". ICoQC 2018. École Normale Supérieure, Paris, France.

Scientific boards and committees

• Scientific board of startup Alice&Bob

• Scientific committee of the quantum information center Sorbonne doctoral school

PhD defense committees

• 2020 : Mario Gely, TU Delft. Invited by Gary Steele.

• 2019 : Romain Albert, CEA Grenoble. Invited by Max Hofheinz.

• 2018 : Iivari Pietikäinen, University of Oulu. Invited by Erkki Thuneberg.

Invited seminars (recent selection)

• Ecole Polytechnique, France. Invited by Timothée Nicolas (2020).

• University of Oulu, Finland. Invited by Erkki Thuneberg (2018)

• University of Berkeley. Berkeley, USA. Invited by Irfan Siddiqi (2018)

• Rigetti Quantum Computing. Berkeley, USA. Invited by Chad Rigetti (2018)

• KIT, Karlsruhe, Germany. Invited by Ioan Pop (2016)

• Néel institute, Grenoble, France. Invited by Nicolas Roch (2016)

• SPEC, CEA Saclay, France. Invited by Daniel Esteve (2016)

Invited conferences (recent selection)

• Neuromorphic meets quantum. C2N Palaiseau France. Invited by Danijela Markovic (2020).

• GDR mésoscopique. Aussois, France. Invited by Bernard Plaçais (2019).

• Quantum cavities. Jouvence, Canada. Invited by Alexandre Blais (2019).

• APS March meeting. Boston, USA. Invited by Blake Johnson (2019)

• ONE-QOS workshop. Max Planck, Erlangen, Germany. Invited by Florian Marquardt (2018)

• IHP workshop on quantum control and feedback, Paris, France. Invited by Eleni Diamanti (2018)

• LIA CNRS-Université de Sherbrooke workshop, Saint-Rémy, France. Invited by Denis Vion (2018)

• APS March meeting. San Antonio Texas, USA. Invited by Eliott Kapit (2015).

Major collaborations

• Raphaël Lescanne at Alice&Bob, France, (quantum computing)

• Mazyar Mirrahimi, Alain Sarlette and Philippe Camapagne-Ibarcq at INRIA Paris, France, (quantum error correction)

• Pierre Rouchon at Mines ParisTech, France, (quantum control)

• Takis Kontos, Matthieu Delbecq and Audrey Cottet at ENS Paris, France, (spin qubits in carbon nanotubes)

• Samuel Deléglise at LKB ENS Paris, France, (optomecanics)

• Emmanuel Flurin at CEA Saclay, France, (microwave photodetection)

• Benjamin Huard at ENS Lyon, France, (quantum error correction)

• Ioan Pop at KIT, Germany, (high kinetic inductance materials)

• Gerhard Kirchmair at University of Innsbruck, Austria, (quantum error correction)

Peer review

• Journal articles: PRL, PRX, Nature Physics.

• Grants: ERC starting grants.

Publications and scientific communications

• **32 published articles** (8 as first author, and 2 as last author), including **4 Nature, 2 Science, 1 Nature Physics (as last author), 2 Phys Rev X, 5 Phys Rev Lett and 3 Nature Comm.**

• **h=16 with 1880 citations** (Thomson/Reuters Web of Science)

Intellectual property

• Patent on a Josephson dipole element that mediates two-to-one photon exchange. With Raphaël Lescanne.

• Patent on a microwave photon detector. With Raphaël Lescanne, Samuel Deléglise and Emmanuel Flurin.

Chapter 2

Introduction

Quantum systems can occupy peculiar states, such as superposition or entangled states. These states are intrinsically fragile and eventually get wiped out by inevitable interactions with the environment. Protecting quantum states against decoherence is a formidable and fundamental problem in physics, which is pivotal for the future of quantum computing. The theory of quantum error correction provides a solution, but its current envisioned implementations require daunting resources: a single bit of information is protected by encoding it across tens of thousands of physical qubits.

My research focuses on protecting quantum information in an entirely new type of qubit with two key specificities. First, it is be encoded in a single superconducting circuit resonator whose infinite dimensional Hilbert space can replace large registers of physical qubits. Second, this qubit is rf-powered, continuously exchanging photons with a reservoir. This approach challenges the intuition that a qubit must be isolated from its environment. Instead, the reservoir acts as a feedback loop which continuously and autonomously corrects against errors. This correction takes place at the level of the quantum hardware, and reduces the need for error syndrome measurements which are resource intensive.

The circuits we develop manipulate quantum states of light, whose utility transcends the long term goal of quantum computing, and can readily be used to probe fundamental properties of matter. In mesoscopic physics where a large number of particles exhibit collective quantum phenomena, the measurement tools to characterize subtle quantum effects are often lacking. My research is also aimed at measuring the spin entanglement of a single Cooper pair, by coupling a superconductor to a circuit composed of microwave resonators and a carbon nanotube. The spin entanglement can be swapped into microwave photons, which can be detected by deploying the arsenal of quantum limited microwave measurement devices.

2.1 Context and motivations

A quantum system interacts with its environment, if ever so slightly, no matter how much care is put into isolating it. The system is progressively revealing its state to its surroundings, resulting in the irreversible destruction of quantum coherence [Haroche and Raimond, 2006]. Nonetheless, during the last half century, immense progress has been made towards extending coherence times by minimizing the sources of noise and their coupling to the system. In the 1980s, the dream of controlling individual quantum systems to boost our computational capabilities was born, but achieving a quantum speedup was hampered by the need for noise levels which were so out of reach that the future of quantum computing seemed doomed. Great hope was reestablished by the theory of quantum error correction (QEC) and its fault-tolerant implementation [Shor, 1996]. In QEC, groups of noisy physical quantum bits (qubits) are arranged together to encode qubits with reduced noise, called logical qubits, and fault-tolerance establishes that noisy quantum computers can operate reliably if the noise is below a threshold. A strong focus in quantum architecture design has been to increase this threshold to a value within experimental reach, but this has come at the price of requiring a daunting hardware overhead: a single logical qubit is encoded across tens of thousands of physical qubits [Fowler et al., 2012]. Therefore, there is a desperate need for new ideas to encode and protect quantum information, and this is the main topic of this proposal.

As a physical platform, I use superconducting Josephson circuits. Unlike microscopic entities such as individual atoms or ions, these circuits are macroscopic arrangements of pieces of superconducting material, assembled in the form of metallic wires and plates [Devoret and Schoelkopf, 2013]. Their state is described by collective degrees of freedom such as voltages and currents, which behave quantum mechanically. Superconductivity and the Josephson effect endow these circuits with low loss and non-linearity, making them ideal systems to engineer complex architectures suitable for quantum information processing.

Over the last few years, together with colleagues, we have developed the theory and experimental implementation of a new paradigm towards quantum computing [Leghtas et al., 2013a, Mirrahimi et al., 2014]. Usually, a qubit is encoded in two energy levels of a system such as an ion or a spin. We took an orthogonal direction. We encoded a logical qubit in a harmonic oscillator [Leghtas et al., 2013a], which has an infinite dimensional Hilbert space, and can therefore replace a register of multiple physical qubits, thus reducing the overhead required for QEC. This paradigm was coined the “cat-qubit” since Schrödinger cat states play

the role of the two qubit states [Vlastakis et al., 2013, Sun et al., 2014]. This led us to reach a landmark in the field of QEC: for the first time, we extended the lifetime of a logical qubit beyond the lifetime of its constituent parts [Ofek et al., 2016]. Up to now, our implementation lacked the key property of fault-tolerance. In a fault-tolerant implementation of QEC, the failure of a single component results in at most a correctable error, a feature which is necessary for scalable quantum computing.

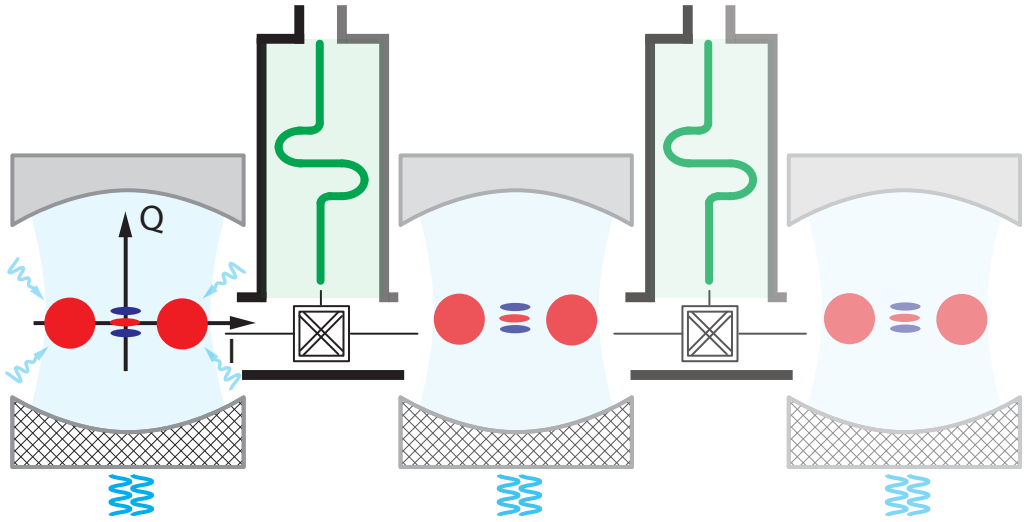

Figure 2.1: Quantum information is encoded in superpositions of Schrödinger cat states (Wigner functions) in high quality cavities (blue). An engineered coupling to a bath (blue waves and dashed mirror) exponentially suppresses bit-flip errors. Exotic circuits (double crossed box), composed of original arrangements of Josephson junctions (JJ) and high kinetic inductance materials, mediate fault-tolerant gates and measurements (green).

My current research focus is to build on these ideas to realize a fault-tolerant logical qubit (see Fig. 2.1). The starting point is to develop a new qubit: unlike others, our qubit is rf-powered, continuously exchanging microwave photons with a reservoir. This approach defeats the natural intuition that a good qubit must be isolated from its environment. Instead, a carefully tailored interaction, (here exchanges of pairs of photons) anchors two steady states which are inherently stable and are therefore ideal to robustly encode quantum information. In this dynamical qubit, as the steady state energy is increased, bit-flips are exponentially suppressed and become negligible in comparison with phase-flips [Mirrahimi et al., 2014, Lescanne et al., 2020]. Such qubits are said to have biased noise and present significant advantages to reduce the overhead for fault-tolerant quantum computing [Aliferis and Preskill, 2008, Webster et al., 2015, Tuckett et al., 2018].

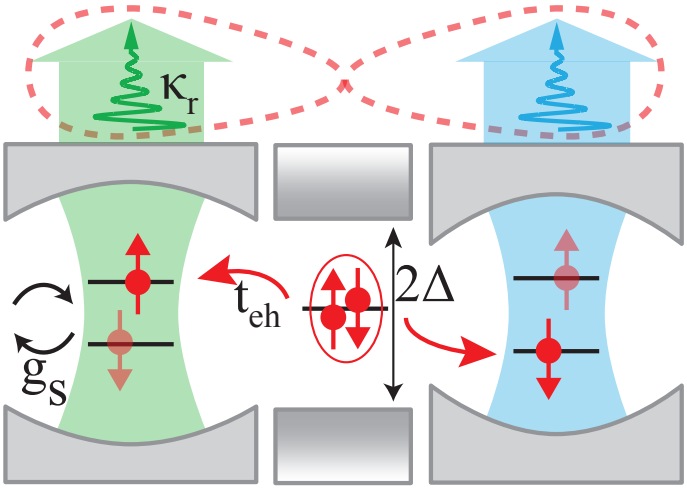

Figure 2.2: A single Cooper pair (CP) in a central superconducting lead (circled pair of spins inside the superconducting energy gap 2Δ), will be spatially split (at rate t_{eh}) into two quantum dots (QD), each embedded in a microwave cavity (green and blue). These QDs will be formed by a carbon nanotube (CNT) (not represented). An engineered spin-photon coupling g_S will swap the CP spin entanglement into two entangled photons propagating at rate κ_r (wavy arrows circled with dashed line) which will be measured with quantum-limited amplifiers (not represented).

The challenge (but also the appeal) of this approach is that it relies on careful tailoring of non-linear interactions, which requires elaborating "exotic" circuits: original arrangements of Josephson junctions (JJ) and new highly inductive materials [Grünhaupt et al., 2018]. These circuits present an interest which transcends their initially envisioned use for quantum computing, and can readily be used to probe fundamental properties of matter with unprecedented precision. As an example, in the Bardeen-Cooper-Schrieffer (BCS) theory of superconductivity, the BCS ground state is a highly entangled state of pairs of electrons, known as Cooper pairs (CP). Although many features of the BCS ground state are observed through effects such as the Josephson effect, the spin entanglement of an individual CP has never been measured. This is why I am insterested in coupling a superconducting lead to a circuit composed of microwave resonators, a carbon nanotube and fermionic reservoirs (see Fig.2.2). A single CP will be isolated into a double quantum dot (QD) formed by a carbon nanotube (CNT), and by synthesizing a strong spin-photon coupling, its spin entanglement will be swapped into microwave photons. Using exquisitely well controlled quantum microwave detectors made of superconducting circuits, we will attempt to detect these photons and quantify the entanglement of a single CP.

By conceiving exotic circuits to first protect quantum information and then probe fundamental properties of matter, my research addresses problems at the boundaries of quantum engineering and fundamental physics. It aims at overcoming the outstanding difficulty of hardware overhead for fault-tolerant quantum computing, and opens the path to probe complex mesoscopic phenomena at the quantum level.

2.2 Early achievements

Encoding and protecting quantum information in a cavity

During my PhD, while I was a visiting student at Yale, I participated in the data analysis of an experiment where we observed Schrödinger cat states [Kirchmair et al., 2013a]. This experience echoed with a parralel project on cat states in which I was envolved with the group of Serge Haroche, Jean-Michel Raimond and Michel Brune [Sarlette et al., 2012]. Inspired by these works, we proposed a new way of encoding and protecting quantum information [Leghtas et al., 2013a], later coined the "cat qubit". The idea was to use the large Hilbert space of a superconducting cavity to redundantly encode information in cat states. This would dramatically reduce the overhead required for error correction. This idea became a major line of research in the groups of Michel Devoret and Robert Schoelkopf at Yale, and led to several pioneering results. First, we encoded information in cat states [Vlastakis et al., 2013], and then repeatedly measured an error syndrome [Sun et al., 2014]. Combining these results, we showed for the first time, that QEC can extend the lifetime of a quantum bit [Ofek et al., 2016]. Thanks to the originality of our approach, we were the first to reach this landmark despite intense competition from large groups like IBM and Santa Barbara.

Stabilizing quantum states by dissipation engineering

During my PhD, we proposed a theoretical protocol to stabilize entangled states of a superconducting circuit [Leghtas et al., 2013b]. This was based on a subtle interplay of coherent drives and dissipation. We showed that although dissipation usually destroys entanglement, if it is combined with carefully tailored couplings, it can instead protect (stabilize) entanglement. A few months later, our protocol was successfully implemented [Shankar et al., 2013]. In parallel, our protocol was declined to efficiently cool a qubit to its ground state [Geerlings et al., 2013].

Protecting and controlling quantum information by dissipation engineering

During my post-doctoral years, we combined the ideas of dissipation engineering and QEC and proposed a new protected (logical) qubit [Mirrahimi et al., 2014]. Our qubit is continuously interacting with its environment through drives and dissipation. This engineered dissipation provides a strong protection against certain error sources, and opens the way towards fault-tolerant qubit gates. A year later, I carried out an experiment showing that is possible

to stabilize not only a single quantum state, but rather a manifold of quantum states [Leghtas et al., 2015], which could then be used to encode quantum information. We then performed coherent oscillations in this manifold [Touzard et al., 2018a]. Finally, we discovered the limitations of our former circuits when subject to strong drives [Lescanne et al., 2019, Verney et al., 2019]. This has guided us towards circuit architectures which circumvent these limitations, leading to the recent observation of the exponential suppression of bit-flips in a cat-qubit [Lescanne et al., 2020].

Five selected publications (Bibliometrics from web of knowledge)

• R. Lescanne, M. Villiers, T. Peronnin, A. Sarlette, M. Delbecq, B. Huard, T. Kontos, M. Mirrahimi and **Z. Leghtas**. *Exponential suppression of bit-flips in a qubit encoded in an oscillator.* **Nature Physics** 16, 509–513 (2020).

• **Z. Leghtas**, S. Touzard, I. M. Pop, A. Kou, B. Vlastakis, A. Petrenko, K. M. Sliwa, A. Narla, S. Shankar, M. J. Hatridge, M. Reagor, L. Frunzio, R. J. Schoelkopf, M. Mirrahimi, and M. H. Devoret. *Confining the state of light to a quantum manifold by engineered two-photon loss.* **Science**, 347(6224):853–857, (2015). **159 citations**.

• M. Mirrahimi, **Z. Leghtas**, V. V. Albert, S. Touzard, R. J. Schoelkopf, L. Jiang, and M. H. Devoret. *Dynamically protected cat-qubits: a new paradigm for universal quantum computation*. **New J. Phys.**, 16(4):045014, (2014). **162 citations**.

• B. Vlastakis, G. Kirchmair, **Z. Leghtas**, S. E. Nigg, L. Frunzio, S. M. Girvin, M. Mirrahimi, M. H. Devoret, and R. J. Schoelkopf. *Deterministically encoding quantum information using 100-photon schrodinger cat states.* **Science**, 342(6158):607–610, (2013). **258 citations**.

• **Z. Leghtas**, G. Kirchmair, B. Vlastakis, R. J. Schoelkopf, M. H. Devoret, and M. Mirrahimi. *Hardware-efficient autonomous quantum memory protection*. **Phys. Rev. Lett.**, 111(12):120501, (2013). **92 citations**.

2.3 Outline of the memoir

This memoir contains a combination of recent, ongoing and future projects in my team. Each one of my three major research themes is described in a dedicated chapter. Chapter 3 focuses on quantum computing with Schrödinger cat states. This has been an ongoing project since my PhD. This effort is led by my PhD students Camille Berdou, Ulysse Rélglade and my former PhD student Raphaël Lescanne (now CTO at quantum computing startup Alice&Bob). Chapter 4 describes a recent and ongoing project on exotic superconducting circuits. It is led by my postdoc Clarke Smith. This chapter contains unpublished preliminary data which, since the time of writing, have been completed and published in [Smith et al., 2020b]. Chapter 5 is a project proposal on a growing interest in my team: using superconducting circuits to probe mesoscopic systems. This work is led by my PhD student Marius Villiers, in collaboration with Takis Kontos, Audrey Cottet and Matthieu Delbecq.

Chapter 3

Quantum computing with Schrödinger cat states

3.1 State of the art

3.1.1 Fault-tolerant quantum computing

Quantum physics has rapidly grown from a theory illustrated with thought experiments, to an experimental discipline where single particles are manipulated in controlled environments [Haroche and Raimond, 2006]. The increasing level of control has nourished the dream of one day using quantum systems to accomplish computational tasks which would outperform current technologies [Nielsen and Chuang, 2000]. However, despite outstanding progress, the residual coupling of quantum systems to their environment (decoherence) and the imprecision in manipulations, has hampered the emergence of quantum machines. The required error rates of operations would need to be so low that they seemed unachievable in any foreseeable future, and therefore, a large scale quantum machine could not be built. Our confidence that these machines could be built was boosted by the theory of quantum error correction (QEC) and its fault-tolerant implementation [Shor, 1996]. Fault-tolerance establishes that in spite of errors, provided they are smaller than a threshold, quantum bits (qubits) can be arranged to run arbitrarily large computations, with arbitrarily low error rates.

The usual approach to QEC is first to list the errors one wants to correct against [Shor, 1995, Steane, 1996, Reed et al., 2012]. Typically, these are uncorrelated single qubit bit-flips, phase-flips, and simultaneous bit-flips and phase-flips (X, Z and Y errors). Then, groups of physical qubits are arranged together to redundantly encode a single quantum bit of information, called

a logical qubit. Well chosen observables (error syndromes) detect whether one of the enlisted errors has occurred, and this information is fed-back to correct the error. The goal is to obtain a logical qubit with a longer lifetime than its constituent physical qubits. This procedure can be concatenated by replacing each physical qubit by a logical qubit, leading to arbitrarily long lifetimes. In order to perform operations (gates) on a logical qubit, the physical qubits need to be manipulated. Fault-tolerance sets a stringent criterion for these gates: during the operation, a single error in any part of the system must result, at most, in a correctable error at the end of the gate. For example, it is imperative that an error on one physical qubit must not result (e.g. through the application of gates), in an extra error on another qubit, which would lead to a correlated error, and since the code was not designed to correct such errors, the logical qubit will be compromised. One of the most outstanding challenges in quantum computing is that currently known fault-tolerant architectures require prohibitive resources: a single logical qubit would need to be encoded over tens of thousands of physical qubits [Fowler et al., 2012]. Today, controlling tens of physical qubits remains a challenge [Otterbach et al., 2017].

3.1.2 Superconducting circuits

My research focuses on a particularly promising physical platform: superconducting circuits. Unlike microscopic entities such as individual atoms or ions, these circuits are macroscopic arrangements of pieces of superconducting material, assembled in the form of metallic wires and plates [Devoret and Schoelkopf, 2013]. The physical dimensions of these pieces translate into distributed capacitances and inductances and the state of the circuit is described by collective degrees of freedom such as voltages and currents, which behave quantum mechanically. Two main ingredients make superconducting circuits appealing for quantum information processing. First, the Josephson junction (JJ), which is formed by two superconducting electrodes (usually aluminum) separated by a thin insulating barrier (usually a few nanometers of aluminum oxide). The JJ endows the circuit with the non-linearity needed to isolate two energy states and form a qubit, without adding dissipation and dephasing. Second: superconductivity, which garantees the frictionless flow of electrical fluid through the metal at low temperature, leading to modes with small dissipation. The possibility to fabricate a wide variety of circuits make them ideal systems to engineer complex architectures suitable for quantum information processing. In the quest of improving the lifetime of superconducting qubits, an active area of research is to improve circuit designs to reduce their sensitivity to decoherence mechanisms, and improve fabrication and materials. This effort has led to a 6 order of mag-

nitude increase in qubit lifetimes in less than two decades [Devoret and Schoelkopf, 2013], rocketing from the nanosecond timescale to milliseconds (quality factors of 10^7). The main sources of decoherence are thought to be dielectric loss at interfaces [Wang et al., 2015] and out-of-equilibrium quasiparticles [Pop et al., 2014, Serniak et al., 2018]. Major progress has been made for the readout of these systems with the development of quantum-limited amplifiers with which we can measure the qubit state about one thousand times per qubit lifetime [Hatridge et al., 2013].

3.1.3 QEC with qubit registers: the surface code

QEC consists in prolonging the coherence of a system by detecting and correcting when errors occur due to an undesired interaction with the environment. This requires redundantly encoding information in a large Hilbert space, which is usually chosen to be the state space of a multi-qubit register. Currently, the surface code [Bravyi and Kitaev, 1998], is the architecture which is under the most serious consideration by several academic and industrial groups [Fowler et al., 2012, Barends et al., 2014, Corcoles et al., 2015, Kelly et al., 2015, Riste et al., 2015]. The surface code model is composed of a large number of identical physical qubits which are connected in a rectangular grid. By having specific linkages between groups of four adjacent qubits, and fast quantum non-demolition (QND) measurements of their parity, the entire grid is protected against errors. This strategy has many appealing properties. It requires a minimum number of different types of elements, and once the development of the elementary cell is successful, the subsequent stages of development might simply be achieved by brute-force scaling. Moreover, its nearest neighbor coupling topology is compatible with planar fabrication techniques, and the allowable error rates are of the order of current performance levels [Barends et al., 2014]. The huge drawback of this approach is that it requires prohibitive resources. Current estimations [Fowler et al., 2012] show that for each logical qubit, one would need of the order of tens of thousands of physical qubits. However, engineering and controlling arrays of more than 10 qubits remains a difficult challenge. My research explores a hardware-efficient approach which could significantly reduce this overhead.

3.1.4 The cat code

The idea of using Schrödinger cat states to encode quantum information was first put forward during my PhD work [Leghtas et al., 2013a]. Since then, this idea has triggered several theoretical and experimental works, which have put the “cat-code” as a serious candidate for

fault-tolerant quantum computing, and is now pursued by several groups around the world at Yale, Sherbrooke, Tsinghua, Chalmers, Stanford and Paris.

Usually, the dominant dissipative processes in an oscillator result from an undesired and uncontrolled interaction with the environment. Examples are energy loss, energy gain due to the finite temperature of the environment, and dephasing due to the random fluctuations of the frequency of the oscillator. These losses are respectively modeled by loss operators $a, a^\dagger, a^\dagger a$, where a is the annihilation operator of the oscillator. These processes lead to decoherence and destroy quantum states such as Schrödinger cat states. Paradoxically, some dissipative processes can actually protect quantum states against some decoherence channels. These processes are naturally very weak, and need to be engineered to become dominant (see methods Sec. 3.3.1). In particular, consider an oscillator which follows the dynamics governed by the loss operator L_2:

$$L_2 = \sqrt{\kappa_2}\left(a^2 - \alpha^2\right) , \tag{3.1}$$

where κ_2 is the rate at which photons are extracted in pairs, usually referred to as the 2-photon dissipation rate and the term in α^2 results from a drive which inserts pairs of photons. This system will force all its states into the two-dimensional manifold [Mirrahimi et al., 2014]

$$\mathcal{M} = \text{span}\{|-\rangle_\alpha, |+\rangle_\alpha\} \approx \text{span}\{|-\alpha\rangle, |\alpha\rangle\} \text{ for large } |\alpha| , \tag{3.2}$$

where where $|\pm\rangle_\alpha = \mathcal{N}_\alpha^+ (|\alpha\rangle \pm |-\alpha\rangle)$, $|\alpha\rangle$ is a coherent state of amplitude α, and $\mathcal{N}_\alpha^\pm = 1/\sqrt{2(1 \pm e^{-2|\alpha|^2})}$ are normalization factors close to $1/\sqrt{2}$ for large $|\alpha|$.

Let's define

$$|0\rangle_\alpha = \frac{1}{\sqrt{2}}\left(|+\rangle_\alpha + |-\rangle_\alpha\right) \approx |\alpha\rangle \tag{3.3}$$

$$|1\rangle_\alpha = \frac{1}{\sqrt{2}}\left(|+\rangle_\alpha - |-\rangle_\alpha\right) \approx |-\alpha\rangle . \tag{3.4}$$

We can then choose to encode quantum information in states of the form (see Fig. 3.1)

$$|\psi\rangle = c_0|0\rangle_\alpha + c_1|1\rangle_\alpha , \tag{3.5}$$

where c_0, c_1 are arbitrary complex numbers satisfying $|c_0|^2 + |c_1|^2 = 1$. Some decoherence processes, such as dephasing (jump operator $a^\dagger a$), result in the state $|\psi\rangle$ diffusing out of the manifold $\mathcal{M}$. On the other hand, the two-photon dissipation process will confine $|\psi\rangle$ in $\mathcal{M}$, and as a result, the dephasing rate κ_φ is exponentially suppressed in the cat size, leading to an effective bit-flip rate $\kappa_X \approx \kappa_\varphi |\alpha|^2 e^{-2|\alpha|^2}$ [Mirrahimi et al., 2014, Appendix A][1].

[1]Our definition of the cat-qubit basis is consistent with [Lescanne et al., 2020] but reversed with respect to

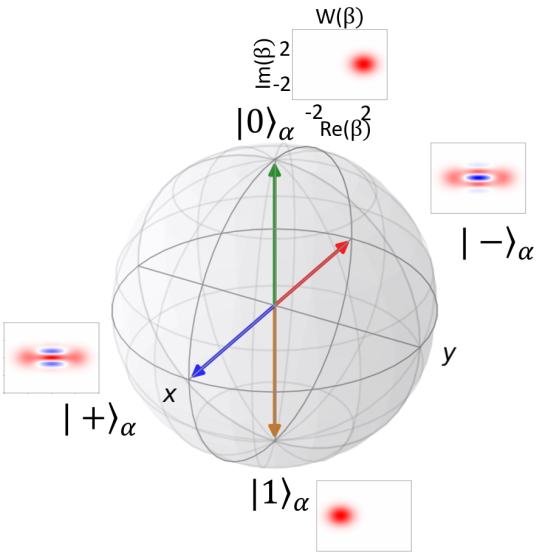

Figure 3.1: The cat-qubit Bloch sphere. Two-photon dissipation defines a set of steady states which form a Bloch sphere, and can encode quantum information. The $|\pm\rangle_\alpha$ states (liying on the x-axis) are coherent states of amplitude $\pm\alpha$ with opposite phases, separated in phase space by the distance $4|\alpha|^2$. As a function of this distance, phase-flips are exponentially suppressed, and bit-flips will be corrected using a standard repetition code.

Error processes, such as single photon loss (jump operator a) which leave $\mathcal{M}$ invariant, need to be corrected differently. Note that $a|+\rangle_\alpha \propto |-\rangle_\alpha$, and $a|-\rangle_\alpha \propto |+\rangle_\alpha$. Hence, photon loss translates into phase-flips. These can be corrected using a simple three cat-qubit repetition code (see Fig.2.1), where the two logical states are

$$\begin{aligned} |0_L\rangle &= |+++\rangle_\alpha \ , \\ |1_L\rangle &= |---\rangle_\alpha \ . \end{aligned}$$

Finally, the confining action of the two-photon dissipation plays a crucial role for fault-tolerant quantum gates. Indeed, the combined effect of a coherent drive and this two-photon dissipation can lead to quantum Zeno dynamics which act as a gate on our protected qubit [Touzard et al., 2018a]. Since the state never leaves the manifold $\mathcal{M}$, if an error occurs, during this gate, it is correctable at the end of the gate.

[Mirrahimi et al., 2014, Grimm et al., 2019]. In the latter references, it is phase-flips which are exponentially suppressed.

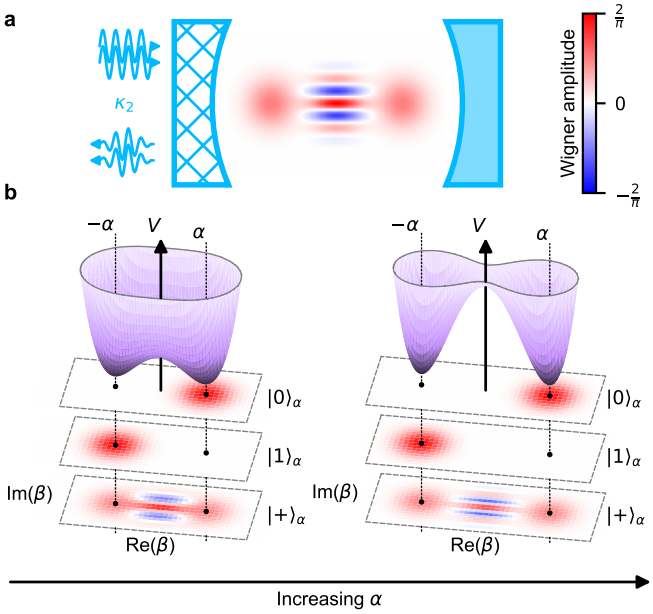

Figure 3.2: **The cat-qubit** (**a**) Quantum information is encoded in a resonator (blue mirrors) coupled to its environment through a special apparatus (hatched mirror) where pairs of photons are exchanged at rate κ_2 (double arrows). (**b**) This dynamics is illustrated by a pseudo-potential V (purple) defined over the resonator quadrature phase space (β plane). The cat-qubit states $|0\rangle_\alpha$ and $|1\rangle_\alpha$ lie in the minima of V and are separated in phase space as shown by their Wigner representations (stacked color plots). Bit-flip errors, which randomly swap $|0\rangle_\alpha$ and $|1\rangle_\alpha$, are exponentially suppressed by increasing this separation. Crucially, this pseudo-potential does not alter quantum superpositions of $|0\rangle_\alpha$ and $|1\rangle_\alpha$ such as the Schrödinger cat state $|+\rangle_\alpha$. *Reproduced from [Lescanne et al., 2020].*

3.1.5 Exponential suppression of bit-flips

In a recent paper [Lescanne et al., 2020], we have measured an exponential decrease of the bit-flip rate as a function of the separation $|\alpha|^2$ between states $|0\rangle_\alpha$ and $|1\rangle_\alpha$, while only linearly increasing the phase-flip rate (errors that scramble the phase of a superposition of $|0\rangle_\alpha$ and $|1\rangle_\alpha$). The bit-flip time reached 1 ms, a 300-fold improvement over the energy decay time of the resonator. This was made possible by inventing a circuit which mediates a pristine non-linear coupling between the resonator and its environment, thus circumventing the problems of previous implementations[Leghtas et al., 2015, Touzard et al., 2018b]. Our qubit combines two unique features: only phase-flips remain to be actively corrected[Tuckett et al., 2018, Tuckett et al., 2019b, Tuckett et al., 2019a, Guillaud and Mirrahimi, 2019], and its 2D phase space can be accessed to perform gates[Mirrahimi et al., 2014, Grimm et al., 2019, Puri et al., 2019, Guil-

laud and Mirrahimi, 2019], making it an ideal building block for scalable fault-tolerant quantum computation with a significant reduction in hardware overhead [Guillaud and Mirrahimi, 2019]. I will now briefly describe this recent result which will serve as a stepping stone for our future projects .

A convenient tool to visualize the semi-classical dynamics of Eq. (3.1) is the pseudo-potential V defined over the complex plane as $-\nabla V(\beta) = \frac{d\beta}{dt}$, where β is the expectation value of a at time t in a semi-classical approximation [Lescanne et al., 2020, Supplement]. Stable steady states are local minima of V (see Fig. 3.2) and correspond to $\beta = \pm\alpha$. An error process can disrupt the stability of these states and induce transitions between them. By analogy with a particle in a double well potential, tunneling (or bit-flips) from one well to another is exponentially suppressed in the separation between the two wells (here defined as $|\alpha|^2$), as long as the error process fulfills two criteria: it has to be local and sufficiently weak. An error process is local if it transforms a state into neighboring states in phase space [Gottesman et al., 2001]. As an example, dominant errors such as photon loss, gain and dephasing are local. Moreover, the effective error rate κ_{err} must be weaker than the confining rate $\kappa_{\text{conf}} = 2|\alpha|^2\kappa_2$ inherited from the confining potential V, in order for the cat-qubit states to remain localized near the potential minima. The outstanding challenge to observe an exponential increase in the bit-flip time is therefore to engineer $\kappa_{\text{conf}} > \kappa_{\text{err}}$ for all dominant local error processes.

Two-photon exchange between a resonator and its environment does not occur spontaneously. Instead, it is synthesized by engineering an interaction that exchanges pairs of photons of the cat-qubit resonator with one photon of an intentionally lossy mode referred to as the buffer[Leghtas et al., 2015]. The interaction Hamiltonian takes the form

$$H_i/\hbar = g_2 a^{\dagger 2} b + g_2^* a^2 b^\dagger \,, \tag{3.6}$$

where b is the annihilation operator of the buffer and g_2 is the interaction strength. Adding a resonant drive on the buffer, we recover Eq. (3.1) with $\kappa_2 \approx 4|g_2|^2/\kappa_b$ and $\alpha^2 = -\epsilon_d/g_2^*$, where ϵ_d is the drive amplitude and κ_b is the buffer energy decay rate, engineered to be larger than g_2[Carmichael, 2007, Leghtas et al., 2015]. Conveniently, the separation $|\alpha|^2$ between the cat-qubit states is readily tunable *in situ* since it is proportional to the buffer drive amplitude.

We have implemented a cat-qubit in a circuit quantum electrodynamics architecture described in Fig. 3.3 operated at 10 mK. It consists of a sputtered niobium film on a silicon substrate patterned into coplanar waveguide resonators. The cat-qubit mode resonates at $\omega_a/2\pi = 8.0381$ GHz, has a single photon lifetime $T_1 = 3.0$ μs limited by leakage to the flux lines [Lescanne et al., 2020, Methods], and is probed through a transmon qubit coupled to a

readout resonator followed by a parametric amplifier. At the flux operating point, the buffer mode resonates at $\omega_b/2\pi = 4.8336$ GHz and has an energy decay rate $\kappa_b/2\pi = 13$ MHz.

It is a technical challenge to engineer the dyanmics of Eq. (3.6) without inducing spurious effects which are detrimental for the protection of quantum information. Examples of such effects are induced relaxation[Sank et al., 2016, Gao et al., 2018], escape to unconfined states [Lescanne et al., 2019, Verney et al., 2019] and quasiparticle generation[Wang et al., 2014]. To mitigate these effects, the interaction of Eq. (3.6) is induced by a novel non-linear dipole: the Asymmetrically Threaded SQUID (ATS, Fig 3.3). The ATS consists of a symmetric SQUID (Superconducting Quantum Interference Device) shunted in its center by a large inductance, thus forming two loops. Here the inductance is built from an array of 5 Josephson junctions. The ATS mediates an interaction of the form $U = -2E_J \cos(\varphi_\Sigma)\cos(\varphi + \varphi_\Delta)$, where E_J is the Josephson energy of the SQUID junctions, φ is the phase across the dipole, and $2\varphi_{\Sigma,\Delta}$ are the sum and differences of flux threading the two loops. We bias the ATS at $\varphi_\Sigma = \varphi_\Delta = \pi/2$, or equivalently, we thread the left and right loops with flux π and 0, respectively. In addition, we drive the sum port with a radio-frequency flux pump $\epsilon(t)$. At this bias point $U = -2E_J \sin(\epsilon(t))\sin(\varphi)$. The ATS is coupled to the buffer and cat-qubit, so that φ is a linear combination of $a, a^\dagger, b, b^\dagger$, and $\sin(\varphi)$ contains only odd powers of these operators. The desired interaction of Eq. (3.6) is present in the expansion of $\sin(\varphi)$, and is resonantly selected by a flux pump frequency $\omega_p = 2\omega_a - \omega_b$[Vrajitoarea et al., 2019]. In contrast with previous strategies[Leghtas et al., 2015, Touzard et al., 2018b], the ATS mediates a pristine two-photon coupling, since Eq. (3.6) is the only leading order non-rotating term, the presence of the inductive shunt prevents instabilities such as the escape of the buffer to highly energetic states[Lescanne et al., 2019, Verney et al., 2019], and the device operates at a first order flux insensitive point (Fig 3.3c). These features are key in order not to introduce inherent error processes that cannot be corrected by two-photon dissipation.

The root advantage of the cat-qubit is that its computational states $|0\rangle_\alpha$ and $|1\rangle_\alpha$ can be made arbitrarily long-lived simply by increasing the cat size $|\alpha|^2$, provided that $\kappa_{\text{conf}} > \kappa_{\text{err}}$. In this experiment, the dominant error is due to energy decay so that $\kappa_{\text{err}}/2\pi = (2\pi T_1)^{-1} = 53$ kHz (Extended Data Figure 1), and $\kappa_{\text{conf}} = 2|\alpha|^2\kappa_2$ with a measured $\kappa_2/2\pi = 40$ kHz (from which we infer $g_2/2\pi = 360$ kHz). Hence, we enter the regime $\kappa_{\text{conf}} > \kappa_{\text{err}}$ as soon as $|\alpha|^2 > 0.7$. We have measured that for each added photon in the cat-qubit state, the bit-flip time is multiplied by 4.2. This exponential scaling persists up to $|\alpha|^2 \approx 3.5$, and the bit-flip time saturates for $|\alpha|^2 \geq 5$ at 1 ms, a 300-fold improvement over the resonator in-

trinsic lifetime (see Fig. 3.4). We expect a saturation when the corrected bit-flip rate reaches the rate of residual errors which are not correctable, such as non-local errors. In the present experiment, we attribute this saturation to the coupling with the transmon employed for the resonator tomography [Lescanne et al., 2020, Supplement], which has a thermal occupation of 1%, a lifetime $T_{1,q} = 5$ μs and is dispersively coupled to the cat-qubit resonator with a rate $\chi_{qa}/2\pi = 720$ kHz. Over a timescale in the millisecond range, the transmon acquires a thermal excitation that shifts the cat-qubit resonator frequency by χ_{qa}. This triggers a rotation of the resonator states which overcomes the confining potential since in this experiment $\chi_{qa} \gg \kappa_{\text{conf}}/2$ [Lescanne et al., 2020, Methods] (note that tomography protocols compatible with smaller values of χ_{qa} have been recently demonstrated[Touzard et al., 2019, Campagne-Ibarcq et al., 2019]). During an average time $T_{1,q}$, the resonator states acquire an angle of order $\chi_{qa}T_{1,q} \gg \pi/2$. When the transmon excitation decays, the rotation stops and the two-photon dissipation brings the resonator state back into the cat-qubit computational basis. By virtue of the dissipative nature of the protection mechanism, this process may result in a bit-flip but does not cause any leakage.

Schrödinger cat states like $|\pm\rangle_\alpha$ living in a resonator with a lifetime T_1, lose their coherence at a rate $2|\alpha|^2/T_1$[Haroche and Raimond, 2006]. In the cat-qubit paradigm, this translates into a phase-flip rate which increases linearly with the cat size $|\alpha|^2$. In addition, our cat-qubit undergoes a flux pump, a drive and non-linear interactions, which could further increase the phase-flip rate. We measure the phase-flip rate for increasing $|\alpha|^2$ and confirm a linear scaling (Fig. 3.5a). Moving towards three dimensional cavities and engineering ever-improving non-linear interactions should decrease the phase-flip rate below a threshold where a line repetition code can actively correct remaining errors [Guillaud and Mirrahimi, 2019].

3.2 Project proposal: a fault-tolerant logical quantum bit

The program of this project is to develop an entirely new way of encoding quantum information, manipulate it in a fault-tolerant manner, and demonstrate the scalability of this approach. The new paradigm we will follow is to correct errors in two stages. First, bit-flips are prevented at the hardware level, continuously and autonomously (no measurements are routed in and out of the system). Second, phase-flips are corrected using a standard 3 cat-qubit repetition code with syndrome measurements and feedback. An operation is said to be fault-tolerant when the failure of one part of the system results at most in a correctable error. In our case, an acceptable error is a single phase-flip on one of the cat-qubits, since it can be corrected by the repetition code.

3.2.1 Observing macroscopic bit-flip times

We have recently observed the exponential decrease of the bit-flip rate between our cat-qubit states $|0\rangle_\alpha$ and $|1\rangle_\alpha$, as a function of their separation in phase space, while only linearly increasing their phase-flip rate [Lescanne et al., 2020]. In this first task, we will improve this result by increasing the lifetime of the cavity to the state of the art of a millisecond [Reagor et al., 2016] and probe the cavity state with a minimally invasive measurement apparatus [Campagne-Ibarcq et al., 2019]. We expect that a cat size of $|\alpha|^2 \approx 5$ (resp. 10) should lead to a macroscopic bit-flip time of $\approx$ 1 second (resp. 0.5 hour), and a phase-flip time of $\approx$ 100 μs (resp. 50 μs). With such a long bit-flip time, the entire effort of active QEC can be focused on correcting the only significant error: phase-flips.

3.2.2 A topologically protected CNOT gate

A crucial step in QEC is to extract information about the encoded system to detect errors. This is achieved by coupling the system to an ancilla which is then measured. Unfortunately, the ancilla itself can fail thus producing an error which can propagate to the encoded system. An error syndrome detector is said to be fault-tolerant when it does not propagate errors on the encoded system beyond those which can be corrected. In this task we will fabricate such a detector. A solution which I find particularly appealing is the proposal of Ref [Guillaud and Mirrahimi, 2019]. It maps the joint parity (syndrome for phase-flips) of two cat-qubits onto an ancilla cat-qubit through two consecutive CNOT gates (see Fig. 3.6). Each CNOT rotates the target in phase space by π if and only if the control is in $|1\rangle_\alpha$ (see Fig. 3.7). This

phase π is robust to small imprecisions in the gate parameters and is therefore described as topological, much like a knot is robust to small distortions of a rope. Remarkably this gate does not convert phase-flips into bit-flips, thus preserving the noise bias. In order to implement this gate, we will employ time-dependent non-linear processes through parametric pumping (see Sec. 3.3.1). We seek to realize the following Lindbladian loss operators:

$$L_{\text{control}} = \sqrt{\kappa_2}\,(a^2 - \alpha^2) \tag{3.7}$$

$$L_{\text{target}} = \sqrt{\kappa_2}\left(b^2 - \frac{1}{2}\alpha(a+\alpha) + \frac{1}{2}\alpha e^{2i\pi t/t_{\text{gate}}}(a-\alpha)\right), \tag{3.8}$$

where a and b are the control and target annihilation operators, t_{gate} is the gate time which needs to be larger than $1/\kappa_2$. We can estimate a fault-tolerant parity measurement rate $\Gamma_m \approx 2\pi \times 100$ kHz, which is two orders of magnitude larger than the intrinsic loss we expect for these resonators $\kappa_1 \approx 2\pi \times 1$ kHz [Kreikebaum et al., 2016].

3.2.3 Three cat-qubit repetition code

We will construct a 3 cat-qubit repetition code, with a joint fault-tolerant parity measurement of cat-qubits 1 and 2, and 2 and 3 (see Fig. 3.8). Since the cat-qubit only suffers from phase-flip errors (bit-flips are exponentially suppressed), this minimal repetition code provides a complete 1st order protection. Thanks to QEC, the lifetime of this repetition code is expected to increase by a factor of the order of $(\Gamma_m/\kappa_Z)/\binom{3}{2} \approx 17$, where $\kappa_Z = |\alpha|^2\kappa_1$ is the phase-flip rate and κ_1 is the resonator energy decay rate (the denominator $\binom{N}{p}$ refers to the number of ways p cat-qubits out of N can flip). If we make fast enough progress, we will build a 5 cat-qubit repetition code, leading to a lifetime improvement of the order of $(\Gamma_m/\kappa_Z)^2/\binom{5}{3} \approx 250$.

3.3 Methods

3.3.1 Parametrically activated non-linear interactions and dissipation

Superconducting circuits have macroscopic degrees of freedom which behave quantum mechanically. A non-linear and non-dissipative element such as a Josephson junction, will provide a non-linear coupling between electro-magnetic modes of the circuit. A typical example is a linear circuit composed of inductors and capacitors, which incorporates a non-linear element (see Fig. 3.8 a-d). The Hamiltonian of such a circuit takes the following form [Nigg et al.,

2012]:

$$H = \sum_m \hbar\omega_m a_m^\dagger a_m + U_{\varphi_{ext}}^{nl}(\varphi)\,, \tag{3.9}$$

$$\varphi = \sum_m \varphi_m \left(a_m + a_m^\dagger\right), \tag{3.10}$$

where ω_m is the frequency of the m^{th} mode, a_m is its annihilation operator, and φ_m is the zero point fluctuation of the phase for mode m. The energy of the non-linear element is denoted $U_{\varphi_{ext}}^{nl}$, where φ_{ext} is the flux threading a loop which the non-linear element may contain. The simplest example is that of JJ: $U_{\varphi_{ext}}^{nl} = -E_J\left(\cos(\varphi) + \varphi^2/2\right)$ [Leghtas et al., 2015], E_J is the Josephson energy. One recognizes the Josephson cosine potential, from which we have subtracted the quadratic part since it is included in the linear Hamiltonian. More generally, $U_{\varphi_{ext}}^{NL} = \sum_{k\geq 3} c_k(\varphi_{ext})\varphi^k$, and the form of the coefficients c_k depends on the circuit topology. A central topic in this project will be to design circuits where certain coefficients c_k dominate others. As an example, let's consider the simple case of a JJ. In the regime where $\|\varphi\| \ll 1$, we expand the cosine term, and all sorts of non-linear coupling terms appear. Some of these terms are always non-rotating, in the sense that they are effective regardless of the frequency difference of modes m and m', or in other words, they are not eliminated by performing the rotating wave approximation. Examples of these terms are:

1. Cross-Kerr terms [Schuster et al., 2007]: they take the form $a_m^\dagger a_m a_{m'}^\dagger a_{m'}$, and can be interpreted as the number of photons in mode m shifting the frequency of mode m', and vice versa.
2. Kerr terms [Kirchmair et al., 2013b] take the form ${a_m^\dagger}^2 {a_m}^2$, and can be interpreted as the number of photons of mode m shifting its own frequency.

More terms can be made non-rotating by driving the circuit with classical drives (see Fig. 3.9), which can be coupled capacitively or inductively (e.g. by modulating φ_{ext}). For simplicity, we will focus on a capacitive coupling. This will effectively displace one of the modes (let's say mode 1), by a scalar term, corresponding to each classical drive, and this scalar will be rotating at the driving frequency [Leghtas et al., 2015]. Hence the phase operator φ in (3.10) is shifted to $\varphi = \sum_m \varphi_m \left(a_m + a_m^\dagger\right) + \varphi_1 \sum_k \left(\xi_k + \xi_k^*\right)$, where ξ_k corresponds to the k^{th} drive. Now a whole variety of terms can be activated by driving the system at well chosen frequencies ω_k. Here are examples of terms one can create.

1. Conversion terms (using three wave mixing: [Teufel et al., 2011, Schackert et al., 2013, Flurin et al., 2015]): they take the form $a_m^\dagger a_{m'} \xi_k^* \xi_{k'}$ + h.c, which represent the con-

version of a photon of mode m into a photon of mode m'. In order to make this term resonant, the two drives k and k' need to have a frequency difference corresponding to the frequency difference of modes m and m': $\omega_k - \omega_{k'} = \omega_m - \omega_{m'}$.

2. Amplification terms (using three wave mixing [Bergeal et al., 2010, Flurin et al., 2015]): they take the form $a_m a_{m'} \xi_k^* \xi_{k'}^*$+h.c, which represent the creation of a pair of photons, one in mode m and one in m'. This occurs when: $\omega_k + \omega_{k'} = \omega_m + \omega_{m'}$.
3. Squeezing term [Kamal et al., 2009]: it takes the form $a_m^2 \xi_k^* \xi_{k'}^* + $ h.c. This term is made resonant by applying two drives at frequencies $\omega_{k,k'}$ such that $\omega_k + \omega_{k'} = 2\omega_m$.
4. Two-photon conversion terms [Leghtas et al., 2015]: they take the form $a_m^2 a_{m'}^\dagger \xi_k^*$+h.c, where two photons from mode m are converted into one photon of mode m'. This term is made resonant by applying a drive at frequency $\omega_k = 2\omega_m - \omega_{m'}$.

Driving a circuit which incorporates Josephson junctions offers a wide range of possibilities to couple modes in a non-linear way, opening the door to a new generation of devices where the outputs depend non-linearly on the inputs, and to quantum simulations with quantum fluids of light [Carusotto and Ciuti, 2013]. In our project, we use these non-linear couplings to generate multi-photon dissipation, as described in the following paragraph.

Let's now assume that in addition to the non-linear couplings described in the previous section, one of the modes, let's say mode 1, is strongly coupled to the environment and dissipates energy at a rate κ_1. If one engineers a coupling of the form $g a_m^n a_1^\dagger$+h.c., where g is the engineered coupling strength, then in the limit where $\kappa_1 \gg g$, this induces an n-photon dissipation process on mode m, at rate $4|g|^2/\kappa_1$. This is derived by adiabatically eliminating mode 1, see for example [Carmichael, 2007, section 12.1],[Leghtas et al., 2015, supp, section 2.3.1]. The result may be generalized to any coupling of the form $g A_m a_1^\dagger$, where A_m is an arbitrary operator acting on mode m, and this will lead to a dissipation process where the jump operator is A_m. As an example we have recently shown that we can achieve two photon dissipation [Leghtas et al., 2015]. It is a technical challenge to achieve large multi-photon dissipation without increasing the natural (single photon) decay rate of the mode. Indeed, if no particular care is taken, the mode could decay directly through the lossy mode it is coupled to, due to the Purcell effect. Engineering circuits where this direct coupling is small will be an important step in our project.

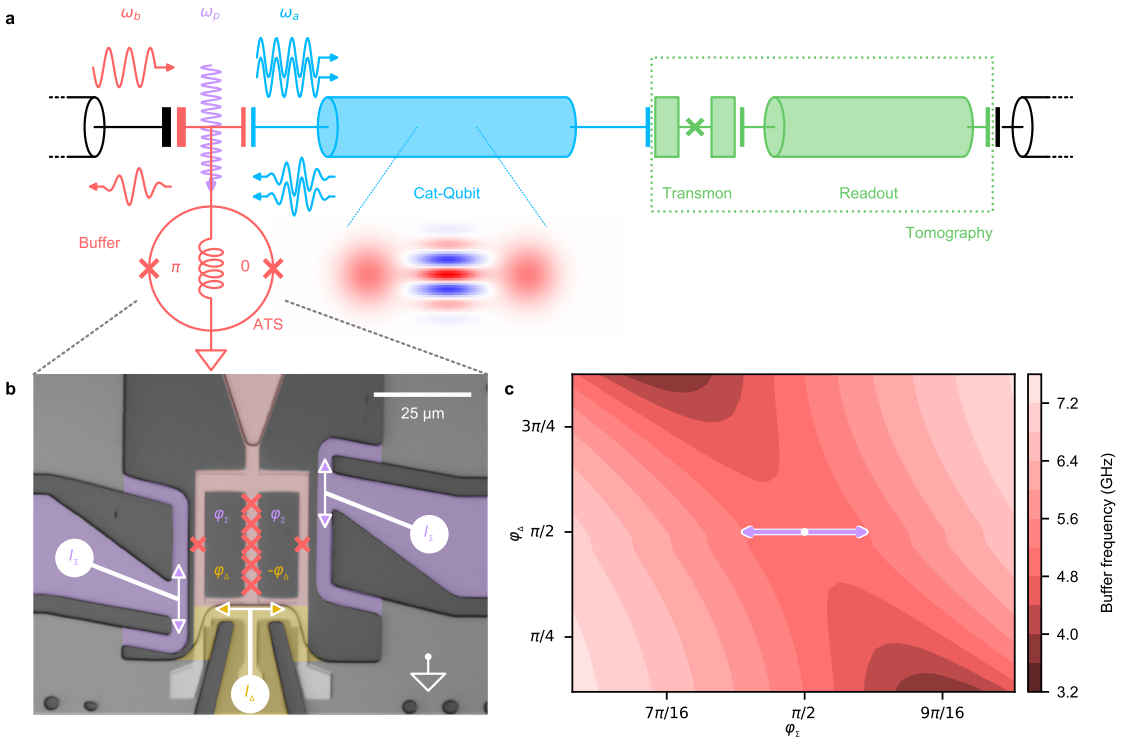

Figure 3.3: **Circuit diagram and implementation** (**a**) The cat-qubit resonator (blue) is coupled on one end to a transmon qubit and a readout resonator (green) to measure its Wigner function, and on the other end to the buffer (red), a lumped element resonator connected to ground through a non-linear element coined the Asymmetrically Threaded SQUID (ATS). The ATS consists of a SQUID shunted by an inductance, forming two loops. Pumping the ATS at frequency $\omega_p = 2\omega_a - \omega_b$ (purple arrow), where $\omega_{a,b}$ are the cat-qubit and buffer frequencies, mediates the exchange of two photons of the cat-qubit (blue arrows) with one photon of the buffer (red arrows) (**b**) False color optical image of the ATS. The shunt inductance is made of an array of 5 Josephson junctions (marked by large red crosses). The left and right flux lines (purple) are connected to the same input through an on-chip hybrid (not represented). They carry the radio-frequency pump and the DC current I_Σ, which thread both loops with flux φ_Σ. The bottom flux line (yellow) carries current I_Δ and threads each loop with flux $\pm\varphi_\Delta$. Combining these two controls, we bias the ATS at the $\pi/0$ asymmetric DC working point. (**c**) Measured buffer frequency (color) as a function of φ_Σ (x-axis) and φ_Δ (y-axis), around the working point $\varphi_\Sigma, \varphi_\Delta = \pi/2, \pi/2$ (white dot). As expected, for $\varphi_\Sigma = \pi/2$ (open SQUID), the buffer frequency does not depend on φ_Δ. We operate the ATS by modulating the flux along the orthogonal direction φ_Σ (purple arrow). From this measurement, we extract all the ATS parameters [Lescanne et al., 2020, Methods]. *Reproduced from [Lescanne et al., 2020].*

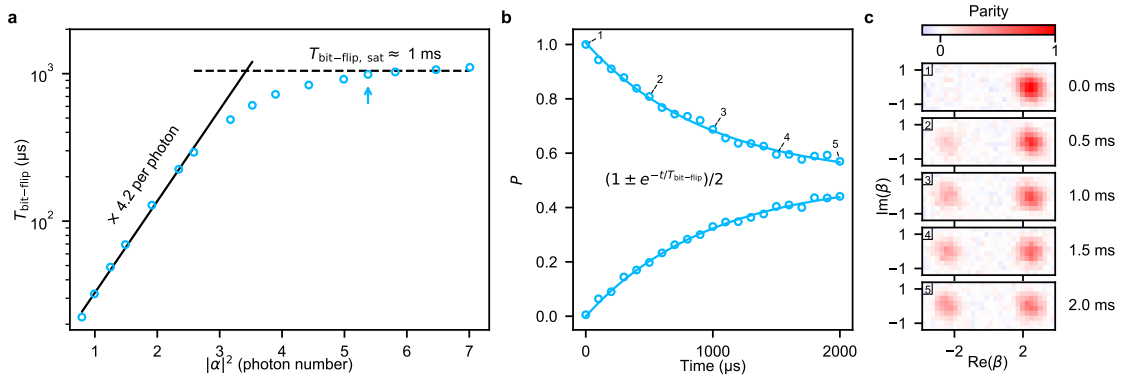

Figure 3.4: **Exponential increase of the bit-flip time with the cat size.** (**a**) The bit-flip time (y-axis) is measured (open circles) as a function of the cat size defined as $|\alpha|^2$ (x-axis). Up to $|\alpha|^2 \approx 3.5$, $T_{\text{bit-flip}}$ undergoes an exponential increase to ≈ 0.8 ms, rising by a factor of 4.2 per added photon (the solid line results from a linear fit of the first 7 data points). The bit-flip time then saturates (dashed line is a guide for the eye) for $|\alpha|^2 \geq 5$ at 1 ms, a factor of 300 larger than the cat-qubit resonator lifetime T_1 in the absence of the pump and drive. Each circle is obtained from measurements such as in (b) for the circle indicated by the blue arrow.. (**b**) The cat-qubit is initialized in $|0\rangle_\alpha$, for a cat size $|\alpha|^2 = 5.4$. After applying the pump and drive for a variable duration (x-axis), the population P (y-axis) of $|0\rangle_\alpha$ (top curve) and $|1\rangle_\alpha$ (bottom curve) is measured. The data (open circles) are fitted to decaying exponential functions (solid lines) from which we extract the bit-flip time. (**c**) Each panel displays the measured normalized Wigner function of the cat-qubit after a pump and drive duration indicated on the right of each plot. Labels 1-5 mark the correspondence with (b). The populations of $|0\rangle_\alpha$ and $|1\rangle_\alpha$ are extracted from the Wigner amplitude at $\beta = \pm\alpha$ respectively, normalized by the amplitude at $+\alpha$ at $t = 0$. The cat-qubit is initialized in $|0\rangle_\alpha$ (top panel) and over a millisecond timescale, the population escapes towards $|1\rangle_\alpha$ (lower panels). The two-photon dissipation ensures that the cat-qubit resonator state remains entirely in the steady state manifold spanned by $|0\rangle_\alpha$ and $|1\rangle_\alpha$. Error bars smaller than the data markers size are not represented. *Reproduced from [Lescanne et al., 2020].*

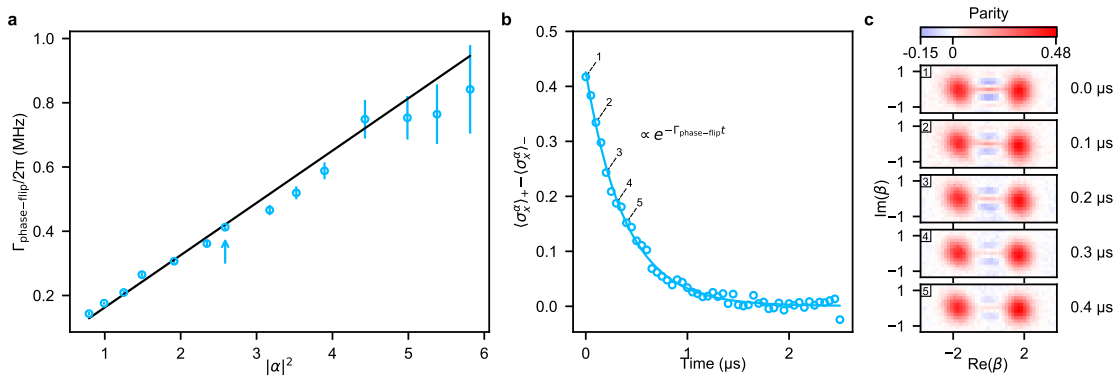

Figure 3.5: **Linear increase of the phase-flip rate with the cat size**. (**a**) The phase-flip rate (y-axis) is measured as a function of the cat size $|\alpha|^2$. The data (open circles) follow a linear trend (the solid line results from a linear fit) as expected for the decay rate of a Schrödinger cat coherence $\Gamma_{\text{phase-flip}} = 2|\alpha|^2/T_{1,\text{eff}}$. We measure $T_{1,\text{eff}} = 2.0\ \mu$s (see error budget in [Lescanne et al., 2020, Methods]), comparable to the intrinsic resonator lifetime of 3.0 μs. Each circle is obtained from measurements such as in (b) for the circle indicated by the blue arrow and the error bars correspond to the uncertainty on the fitting parameter. (**b**) The cat-qubit is prepared in the initial states $|\pm\rangle_\alpha$, for a cat size $|\alpha|^2 = 2.6$. After applying the pump and drive for a variable duration (x-axis), $\langle\sigma_x^\alpha\rangle_\pm$ is measured for each initial state and the difference is represented on the y-axis. The X Pauli operator of the cat-qubit σ_x^α corresponds to the photon number parity. The data (open circles) are fitted to a decaying exponential (solid line) from which we extract the phase-flip rate. (**c**) Each panel displays the measured normalized Wigner function of the cat-qubit after a pump and drive duration indicated on the right of each plot. Labels 1-5 mark the correspondence with (b). The cat-qubit is initialized in the $|+\rangle_\alpha$ state and the positive and negative fringes demonstrate the quantum nature of this initial state (top panel). The fringe contrast is reduced by single photon loss which mixes $|+\rangle_\alpha$ with $|-\rangle_\alpha$. Error bars smaller than the data markers size are not represented. *Reproduced from [Lescanne et al., 2020].*

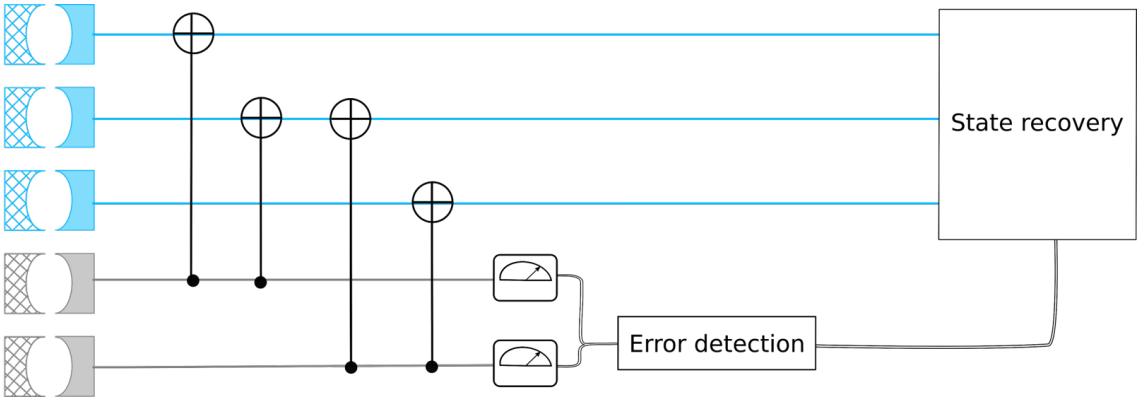

Figure 3.6: **Circuit for the detection of phase-flips in a three cat-qubit repetition code**. Three data cat-qubits (blue) are coupled to two ancilla cat-qubits (grey). The data qubits store quantum information in the basis $\{|+++\rangle_\alpha, |---\rangle_\alpha\}$. The ancilla qubits are prepared in the $|{+}{+}\rangle_\alpha$ states. Each CNOT maps the parity of the target (data) to the control (ancilla). Indeed a CNOT on control and target acts as follows $|{+}{+}\rangle_\alpha \rightarrow |{+}{+}\rangle_\alpha$ and $|{+}{-}\rangle_\alpha \rightarrow |{-}{-}\rangle_\alpha$. Hence, two consecutive CNOT gates map the joint parity of two targets onto the control, which is then measured in the $\pm$ basis. The ancilla measurements unravel whether a phase-flip has occured on the data, maintaining the purity of the encoded information. The entire cycle is repeated over time.

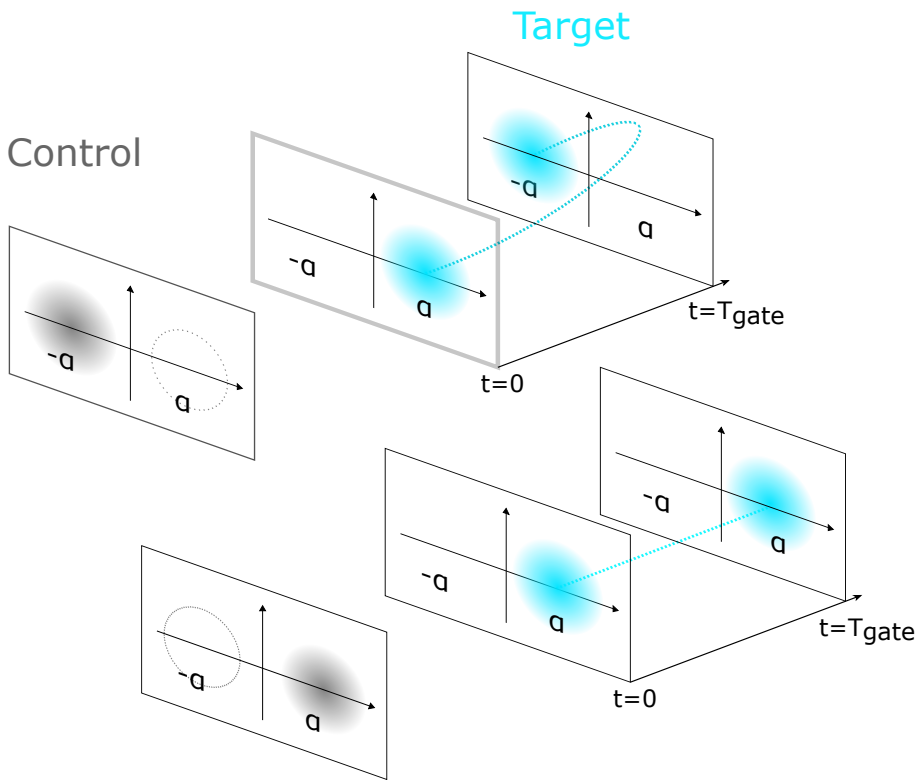

Figure 3.7: **CNOT gate between two cat-qubits**. Each panel represents the Wigner function of the target and control cat-qubits in their computational states. In this basis, the control remains unchanged. The target rotates in phase space from time $t = 0$ to the total gate time $t = T_{\text{gate}}$ by π if and only if the control is in $|1\rangle_\alpha \approx |-\alpha\rangle$. The two-photon pumping is on at all times during the gate, and since the target loops around phase space, distances between computational states are maintained at all time. Moreover, a phase-flip occuring at any time is not converted into a bit-flip. Consequently, we do not loose the protection against bit-flips, and this gate is said to preserve the bias of the noise.

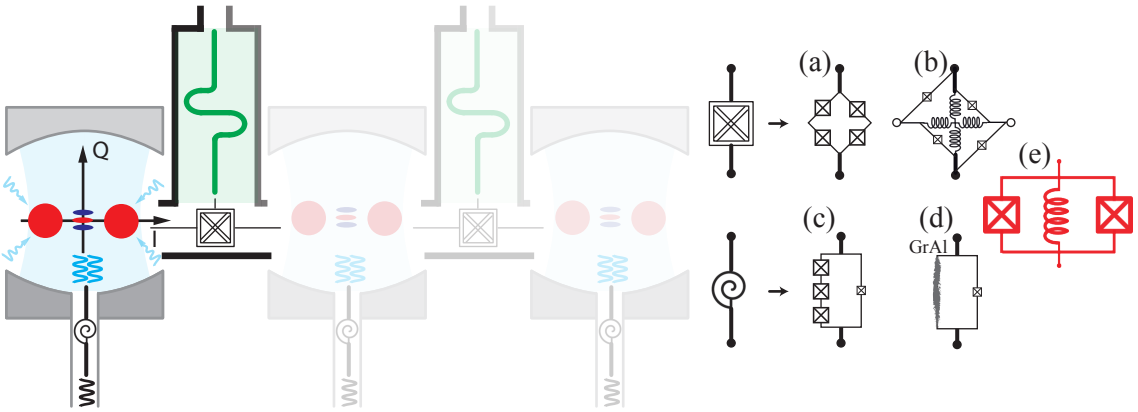

Figure 3.8: Quantum information is encoded in superpositions of Schrödinger cat states (Wigner functions) in high quality cavities (blue). By coupling these cavities to each other and to photonic baths with carefully tailored interaction couplings, we will demonstrate a fault-tolerant logical qubit. These couplings are mediated by exotic circuits: element in the form of a snail (so-called SNAIL [Frattini et al., 2017]), and the double crossed box [Cohen et al., 2017]. During this project, we will use and improve these circuits to obtain the purest desired interactions (e.g $a^2b^\dagger, \cos(2|\alpha|(a+a^\dagger))$), while reducing parasitic coupling terms which can induce errors (e.g. $a^\dagger a b^\dagger b$), where a and b are the annihilation operators of the cat-qubit (of amplitude α) and reservoir resonators respectively. Examples of these circuits are shown: (a) a rhombus [Douçot et al., 2005], (b) an asymetric Josephson ring modulator [Mirrahimi et al., 2014], (c) a SNAIL element, (d) a JJ shunted by a superinductance made of granular Aluminum (GrAl) [Grünhaupt et al., 2018], (e) our newly invented asymetrically threaded squid (ATS) [Lescanne et al., 2020].

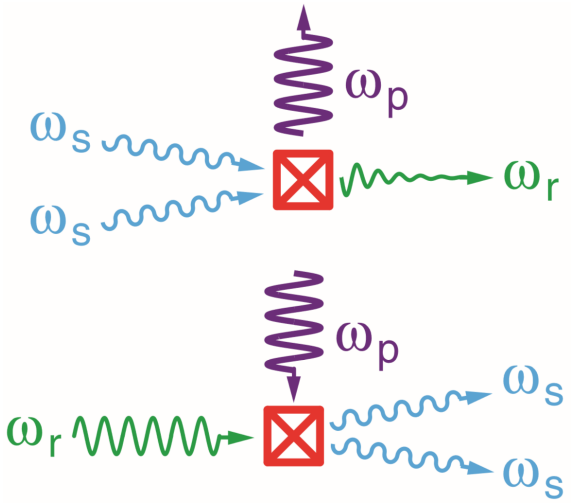

Figure 3.9: Parametric pumping: a non-linear element (red box) is driven with a pump (purple wave), thus inducing a desired non-linear process between modes, here: the exchange of pairs of photons from one mode (blue) to another (green). Figure from [Leghtas et al., 2015].

Chapter 4

Exotic superconducting circuits

4.1 State of the art

4.1.1 The Cooper pair box, the Transmon and the Fluxonium qubits

Superconducting qubits are arrangements of (i) wires where currents can flow, (ii) plates where electric charge can accumulate, and (iii) thin insulating barriers through which charges can tunnel. These three ingredients act respectively as inductors, capacitors and Josephson junctions. The energy scales attributed to these elements are respectively the inductive energy E_L, the charging energy E_C and the Josephson energy E_J. A general single-degree-of-freedom superconducting qubit, represented in Fig. 4.1, has the following Hamiltonian

$$H = 4E_C(N - N_g)^2 + \frac{1}{2}E_L(\varphi - \varphi_{\text{ext}})^2 - E_J \cos(\varphi) \,, \tag{4.1}$$

where N is the operator corresponding to the number of tunneled Cooper pairs, and φ its conjugate phase operator. The charge offset and external flux are denoted N_g and φ_{ext}. Over the last 20 years, a remarkable number of superconducting qubits have been invented by varying the two ratios E_J/E_C and E_L/E_J [Girvin, 2011, Devoret and Schoelkopf, 2013, Smith, 2020]. As an example, the Cooper pair box corresponds to $E_J/E_C < 1$ and $E_L/E_J = 0$ (i.e the inductor is replaced by an open). The Transmon operates in the regime where $E_J/E_C \gg 1$ (typically 50), and again the inductor is an open circuit. The Fluxonium operates at $E_J/E_C > 1$, and $E_L/E_J \ll 1$. Sensitivities to various noise sources and intrinsic properties such as anharmonicity vary from one circuit to another.

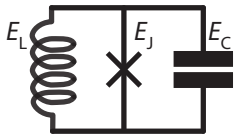

Figure 4.1: General single-degree-of-freedom superconducting qubit.

4.1.2 Exotic circuits with enhanced lifetimes

Let's start by describing some original approaches to fault-tolerant quantum computing, starting with topological codes [Kitaev, 2003] where information is encoded in non-abelian anyons, and gates are performed by braiding. The search for particles with anyonic statistics is an active area of research, and their usefulness for quantum computing is still at an exploratory stage. However, recent works have shown that using Josephson circuits, one can mimic the properties of a topological qubit, by obtaining two states which are spatially separated in phase space, and with an energy difference which is exponentially small in the system size. A prominent example is the so-called "0-π" qubit which seems promising to robustly encode quantum information [Douçot and Vidal, 2002, Ioffe and Feigel'man, 2002, Kitaev, 2006, Brooks et al., 2013]. The groups led by D. Schuster and J. Koch are working on the experimental implementation of this idea [Groszkowski et al., 2018]. Another direction is to design circuits which decouple from noise mechanisms by virtue of special symmetries in the circuit at specific bias points. Recently, the group led by V. Manucharyan in Maryland, has fabricated a device incorporating a SQUID (superconducting quantum interference device) shunted by a superinductance (formed by an array of JJs), and by biasing the circuit with a DC magnetic flux, dominant decay mechanisms are suppressed, leading to an impressively long decay time in the millisecond range [Lin et al., 2018].

4.1.3 High impedance circuits

Achieving strong couplings between modes is a pre-requisite to probe and protect quantum states of light and matter. The electrical coupling to an LC resonator mode scales with its impedance. This holds for two resonators coupled through a JJ and for a resonator coupled to a QD. The impedance $Z = \sqrt{L/C}$ of a resonator is said to be large when it exceeds the impedance quantum $Z_Q = \hbar/(2e)^2 \approx 1$ kΩ. High impedance resonators require small capacitance and very large inductance; the latter is known as a superinductance. For fundamental reasons (fine structure constant much smaller than unity), superinductances are not easy to

fabricate with geometric inductances [Manucharyan, 2012], although this has recently become possible with spiral resonators [Peruzzo et al., 2020] (also developped in the groups of Gary Steele, Fabien Portier, Max Hofheinz and others). One well-known non-geometric contribution to the inductance originates from the inertia of the charge carriers, the so-called kinetic inductance. Recent experiments have proposed and demonstrated several new techniques based on: arrays of JJ [Manucharyan et al., 2009, Masluk et al., 2012], atomic layer deposition [Shearrow et al., 2018], oxidized aluminum grains [Grünhaupt et al., 2018] (see Fig. 4.2), high kinetic inductance of NbTiN [Bruno et al., 2015], and most interestingly for this project, the development of an original arrangement of JJs which doubles the phase fluctuations across the circuit, giving rise to an element coined the "cos(2φ)" junction [Douçot and Vidal, 2002, Gladchenko et al., 2008, Smith et al., 2020a].

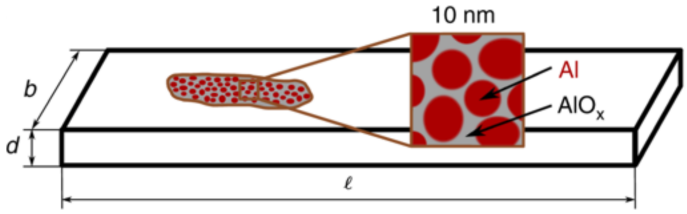

Figure 4.2: Schematic representation of a granular Aluminum stripline resonator. Typical dimensions are $l \approx 2$ mm, $b \approx 3$ μm, $d \approx 20$ nm. Al grains (bordeaux color) have a diameter of a few nm. They are separated by aluminum oxide barriers (shown in gray), forming a 3D network of superconducting islands connected by Josephson contacts. Figure from [Maleeva et al., 2018].

4.2 Project proposal: synthetic high impedance via circuit engineering[1]

It is convenient to rewrite Eq. 4.1 in the following form

$$H = \hbar\omega a^\dagger a - E_J \cos(\varphi_{\text{zpf}}(a + a^\dagger) - \varphi_{\text{ext}}) \,, \tag{4.2}$$

where $\hbar\omega = \sqrt{8E_L E_C}$ and $\varphi_{\text{zpf}} = \left(\frac{2E_C}{E_L}\right)^{1/4} = \sqrt{Z/2Z_Q}$. The annihilation and creation operators a and $a^\dagger$ were introduced such that $\varphi = \varphi_{\text{zpf}}(a + a^\dagger)$. This Hamiltonian now resembles that of a harmonic oscillator perturbed by a Josephson potential.

[1]Since the time of writing, this work has been published in Ref [Smith et al., 2020b]

The regime where phase fluctuations of the resonator across the JJ exceed unity: $\varphi_{\text{zpf}} > 1$, has been out of reach until very recently. This regime has promising applications for protected qubits [Brooks et al., 2013] and fault-tolerant error syndromes [Cohen et al., 2017].

A recent experiment [Pechenezhskiy et al., 2019] has accomplished a nano-fabrication tour-de-force by suspending an array of 460 JJs above the Si substrate. In this configuration, the electromagnetic mode is in vacuum rather than Silicon which has a relative permittivity of ≈ 11.7, leading to an increase in the circuit impedance.

In this project, we enter the regime where $\varphi_{\text{zpf}} > 1$ by circuit engineering: we replace the JJ by an exotic circuit coined the $\cos(2\varphi)$ element [Smith et al., 2020a] (see Fig. 4.4). This circuit contains two JJs in parallel, each in series with inductances of energy $2\epsilon_L$. These elements form a loop threaded by flux ϕ_{ext}. The theoretical prediction is that this circuit has the following Hamiltonian at $\phi_{\text{ext}} = 0, \pi$:

$$H_{\phi_{\text{ext}}=0} = \hbar\omega_0 a^\dagger a - E_{J,0}\cos(\varphi_{\text{zpf},0}(a+a^\dagger) - \varphi_{\text{ext}}) \tag{4.3}$$

$$H_{\phi_{\text{ext}}=\pi} = \hbar\omega_\pi a^\dagger a - E_{J,\pi}\cos(2\left(\varphi_{\text{zpf},\pi}(a+a^\dagger) - \varphi_{\text{ext}}\right)), \tag{4.4}$$

where $\omega_\pi = \omega_0/\sqrt{2}$, $E_{J,\pi} = E_{J,0}$ and $2\varphi_{\text{zpf},\pi} = 2^{3/4}\varphi_{\text{zpf},0}$. Note that the effective zero-point-fluctuations have gained a factor $2^{3/4}$, leading to an effectively increase in the impedance by a factor $2^{3/2} \approx 2.8$.

We verify this prediction by a spectroscopy measurement. First, a calibration experiment (Fig. 4.6) maps the controls (I_x, I_y) to the two Hamiltonian parameters $(\varphi_{\text{ext}}, \phi_{\text{ext}})$. Then, through two-tone spectroscopy, we measure the circuit transition frequency as a function of φ_{ext} for $\phi_{\text{ext}} = 0$ and $\phi_{\text{ext}} = \pi$ (see Fig. 4.7). We observe, as expected, a significant flattening of the first transition energy as a function of φ_{ext}. By fitting this data to the model of Eq. (4.2), we find that the zero-point-fluctuations of the phase are increased from 1.95 to 3.56.

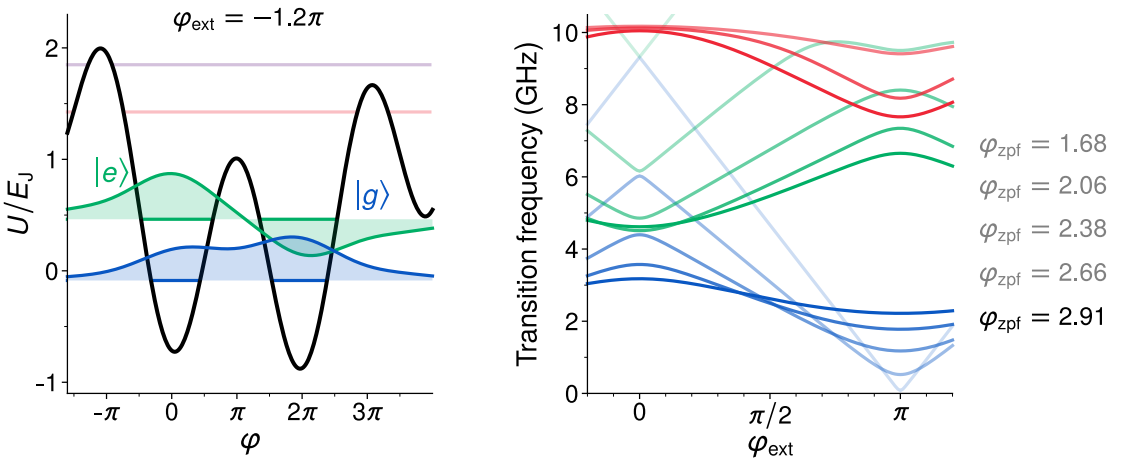

Figure 4.3: **Energy levels of a Fluxonium qubit**. (Left) Potential energy U and the lowest energy levels at $\varphi_{ext} = -1.2\pi$. (Right) Three lowest transition energies (blue, gree, red) for various φ_{zpf}, keeping the central lowest resonance constant. As φ_{zpf} exceeds unity, the flux dependence of the lowest energy transition is washed out.

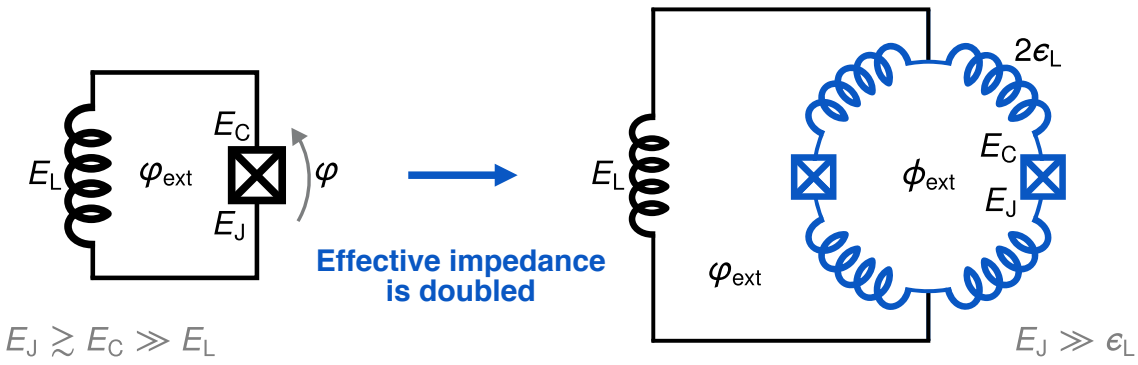

Figure 4.4: **The** $\cos(2\varphi)$ **Fluxonium**. (Left) a typical Fluxonium qubit. (Right) The JJ is replaced by a dipole (blue) composed of an exotic arrangement of two JJs and four inductors. At $\phi_{ext} = \pi$, this dipole energy is $\cos(2\varphi)$ where φ is the phase across the dipole (rather the $\cos(\varphi)$ for a JJ).

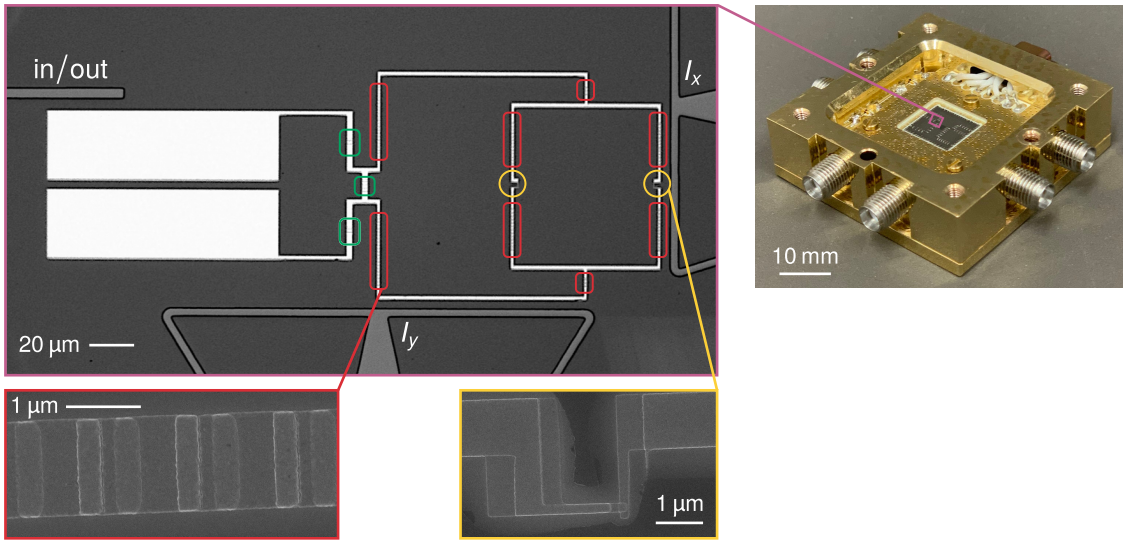

Figure 4.5: **Picture of sample**. (Top left) Optical image of the cos(2φ) Fluxonium (light gray, Aluminum) and its flux bias lines (dark gray, Nb). The substrate is Silicon. The left plates are antenna pads (not represented in Fig. 4.4) to readout this qubit through the in/out port. (Bottom left) SEM image of 7 of the ≈100 JJs forming the superinductor of energy E_L. (Bottom right) SEM image of one of the 2 JJs forming the cos(2φ) element. (Right) Sample holder housing the chip.

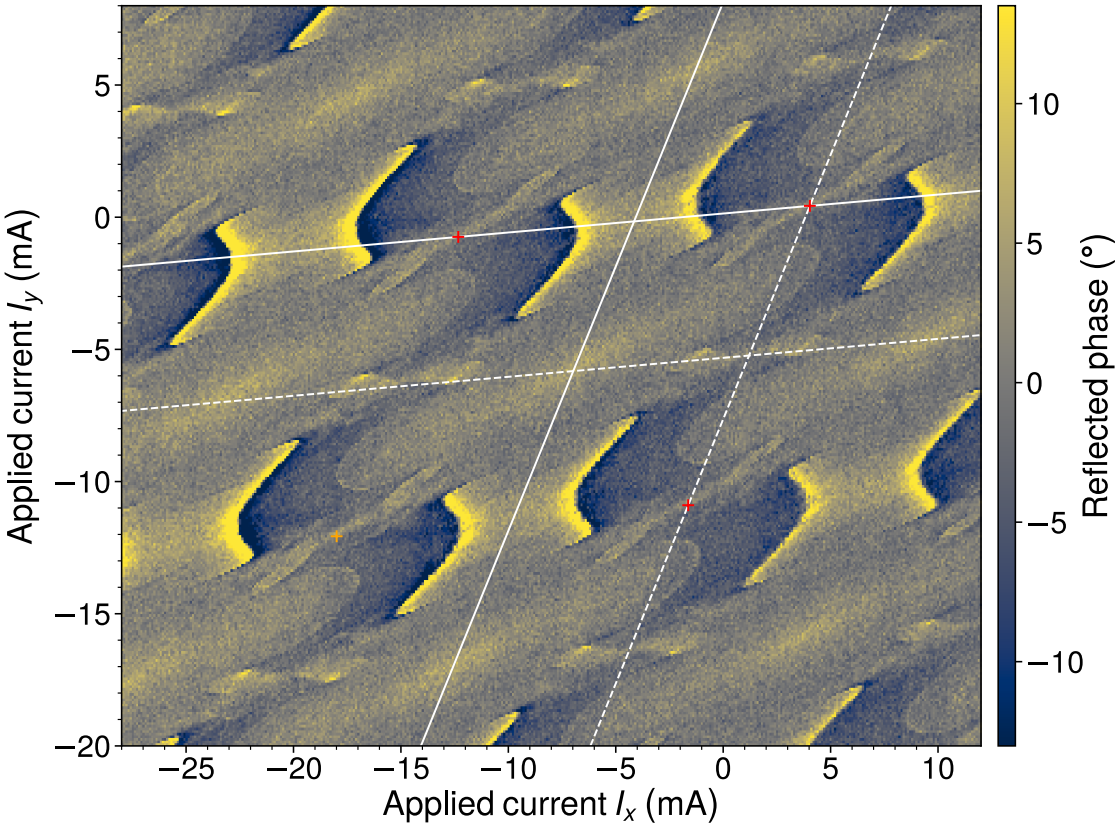

Figure 4.6: **DC bias calibration.** Phase of the reflected signal at the antenna frequency (color) as a function of the DC currents I_x and I_y flowing through the two ports depicted in Fig. 4.5. Guides to the eye show the tilted axis corresponding to φ_{ext} and ϕ_{ext}

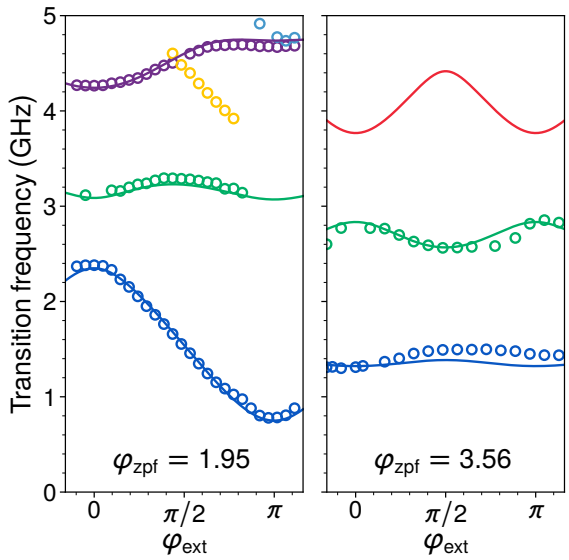

Figure 4.7: **Sensitivity to flux washed out by zero-point-fluctuations.** Measured circuit transition frequencies (open circles) and corresponding fits (full lines) as a function of φ_{ext} (x-axis). The circuit is operated at $\phi_{ext} = 0$ (left) and $\phi_{ext} = \pi$ (right).

Chapter 5

Quantum sensing of a mesoscopic system

My research focuses on using superconducting circuits not only to robustly encode quantum information, but also to probe fundamental properties of mesoscopic systems.

5.1 State of the art

5.1.1 Mesoscopic quantum electrodynamics

A system is said to be *mesoscopic* if its dimension is much larger than the size of the atoms which compose it, but small enough for quantum effects to emerge. This usually implies systems with dimensions in the micrometer range which are fabricated in clean room facilities, and temperatures below 1 Kelvin which are cooled down in dilution refrigerators. In mesoscopic systems, electrons behave as waves and not merely as point-like particles, and can display a rich variety of physical phenomena such as the Aharonov-Bohm effect. A typical example of a mesoscopic system is a quantum dot (QD) [Kouwenhoven et al., 2001]. QDs are zero dimensional objects meaning that their size is constrained in the three spatial dimensions: height, length and width. QDs play the role of electron boxes, where electrons occupy quantum states consistent with the boundary conditions imposed by the box. They can be realized starting from higher-dimensional objects, provided that electrodes are used to ultimately confine electrons in small volumes.

The most common way to probe these systems is through DC transport measurements. A voltage bias is applied and a current is measured, and relevant parameters are varied such

as gate bias voltages and magnetic fields. Recently, mesoscopic systems have been embedded in photonic cavities and probed with microwaves, starting the emergent field of mesoscopic quantum electrodynamics (QED) [Delbecq et al., 2011]. Initially, the motivation was to mediate couplings between distant QDs for quantum information processing [Childress et al., 2004]. The goal of mesoscopic QED then expanded to using microwave as a complementary probe of mesoscopic systems [Desjardins et al., 2017, Hays et al., 2018, Tosi et al., 2019]. First, DC transport necessitates to couple the system to electrodes, making it an open quantum system which exchanges particles with its environment. This coupling leads to decoherence and can damp quantum signatures. In contrast, microwave photons can non-destructively interact with the system electrons, which can be completely isolated from their electrodes. Second, microwave measurements provide complementary information to DC measurements. For example, in the Kondo regime, microwave measurements revealed that the Kondo conduction peak is not accompanied by charge fluctuations in the QD [Desjardins et al., 2017], demonstrating a long-standing theoretical prediction. In the same spirit, we are building an experiment to detect the entanglement of a single Cooper pair by extracting it from a mesoscopic superconducting lead into two QDs, and swapping the spin entanglement into entangled propagating microwave photons.

5.1.2 Carbon nanotubes

We will use carbon nanotubes (CNT) [Laird et al., 2015] as a base material for our mesoscopic system. A CNT is a rolled up graphene sheet, with a diameter of a few nanometers, and lengths as long as a few microns. Due to the small radial dimension, a CNT is an almost ideal one dimensional conductor, which has been shown to grow exceptionally cleanly, leading to low inherent disorder [Cao et al., 2005]. Moreover, the micron length of a CNT makes it possible to control the potential at each point along its length using an array of transverse electrostatic gates [Waissman et al., 2013]. These gates are used to confine electronic states in the longitudinal dimension, and to tune, in-situ, their coupling to fermionic reservoirs. A particularly attractive feature of CNTs, is that they can be stapled [Waissman et al., 2013] on a wide variety of circuits, and in particular, high quality superconducting circuits [Cubaynes et al., 2019] incorporating JJs. In this project, we will use a CNT to form two quantum dots, which will each hold one electron of a split Cooper pair.

5.1.3 Probing spins with photons

Many groups around the world have achieved or are pursuing the strong coupling of a single spin to the electromagnetic mode of a cavity. This task is challenging because the natural coupling of a spin to the magnetic part of the electromagnetic field is weak [Tosi et al., 2014]. One route is to increase this coupling by confining the microwave field in a constriction of nanometric dimensions [Haikka et al., 2017, Bienfait et al., 2016]. Another route is to hybridize the spin and the charge in order to benefit from the strong charge coupling but without significantly degrading spin coherence [Childress et al., 2004]. Recently, strong coupling of a single spin to a single photon has been achieved in a Silicon double quantum dot with micromagnets [Samkharadze et al., 2018, Mi et al., 2018], and in a CNT using the proximity effect of two non-collinear ferromagnetic leads [Cottet and Kontos, 2010, Cubaynes et al., 2019]. We will borrow the ideas from all these works to enhance the spin-photon coupling, using in particular a CNT with ferromagnetic leads and high impedance microwave resonators.

5.2 Project proposal: Measuring the entanglement of a single Cooper pair

In parallel to the increasingly exquisite control we have over superconducting circuits, important developments in the nanofabrication of CNT devices have been made [Waissman et al., 2013], letting us envision experiments which would have been out of reach a few years ago. I will now a describe our plan to measure the spin entanglement of a single Cooper pair (see Fig. 5.1).

5.2.1 Coherent swap of a single Cooper between a superconductor and a double QD

When a superconductor is connected to a double QD at a distance smaller than the superconducting coherence length, it has been predicted that a single Cooper pair (CP) can coherently tunnel from the superconductor into the two quantum dots, forming a spatially separated singlet state [Recher et al., 2001]. The coherence of this singlet state depends on two ingredients: first the coherence of the splitting process itself, and then the dephasing time of the double QD. Regarding the latter point, we have recently obtained promising dephasing times in a CNT double QD [Cubaynes et al., 2019]. The former point is due to the fact that CP injection

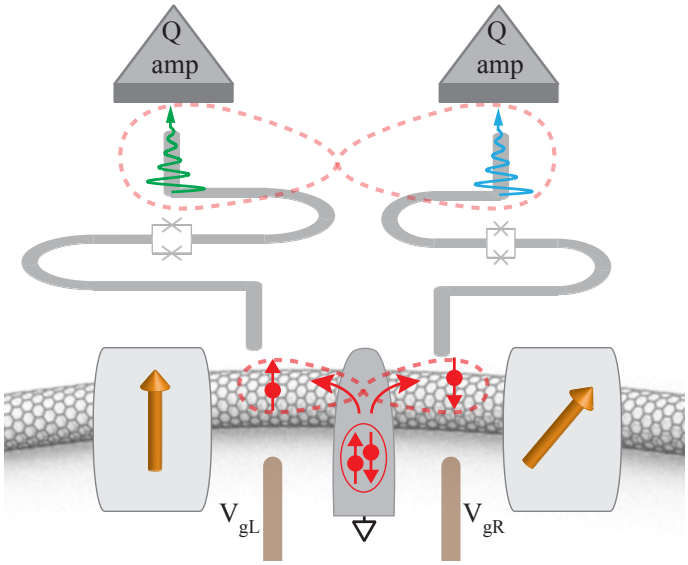

Figure 5.1: Principle for the detection of the spin-entanglement of a single Cooper pair. A mesoscopic superconductor (central lead) is galvanically coupled to a CNT which forms two QDs. A coherent hopping term transfers a single Cooper (circled pair of spins) to the QDs. Lateral non-colinear ferromagnetic electrodes (boxes with arrows), induce a spin-photon coupling between the QDs and their neighboring superconducting resonator (gray meanders). These resonators will be frequency tunable by threading magnetic flux through a SQUID (crosses). The resonator will induce spin flips and transfer the spin-entanglement to two propagating photons (blue and green wavy lines), which will be detected with state of the art quantum limited amplifiers (triangles). The entire sequence will be governed by gate voltages V_{gL}, V_{gR} (brown lines).

is due to a coherent cross Andreev reflection which induces a coherent coupling t_{eh} between the state where the CP is in the superconductor and the state where the CP is in the double QD. The goal of this task is to experimentally verify that this splitting is coherent and measure its strength. Using gate voltages, we have an in-situ control of the chemical potential of the left and right QD: ϵ_L, ϵ_R. By sweeping their sum value $\epsilon_\Sigma = \epsilon_L + \epsilon_R$ through the chemical potential of the superconductor μ_S, we effectively sweep the energy of the singlet $|S\rangle$ state through the energy of the unoccupied state $|\varnothing,\varnothing\rangle$ (see Fig. 5.2). At resonance $\epsilon_\Sigma = \mu_S$, since the superconductor induces a coupling between $|\varnothing,\varnothing\rangle$ and $|S\rangle$, we should observe an energy splitting whose magnitude is precisely $2\sqrt{2}t_{eh}$. We denote $|V_1\rangle$ and $|V_2\rangle$ the two corresponding eigenstates. I now explain how we plan to measure this avoided crossing. Since we are interested in the regime where the DQD is closed, transport measurements will provide weak

signals. I will follow the proposal of Ref. [Cottet, 2012] which uses a microwave cavity. The cavity photons couple $|V_1\rangle$ to $|V_2\rangle$. Employing a two-tone spectroscopy, we expect that when we drive the $|V_1\rangle$ to $|V_2\rangle$ transition, we observe a frequency shift on the cavity. This shift verifies $\chi = {g_C}^2/\Delta$, where g_C is the cavity to QD coupling $g_C \approx 2\pi \times 25$ MHz [Cubaynes et al., 2019], and Δ is the detuning between the cavity and the $|V_1\rangle$ to $|V_2\rangle$ transition, which lies in the GHz range. This leads to a shift in the MHz range, comparable to the linewidths of our cavities, so this shift should be observable.

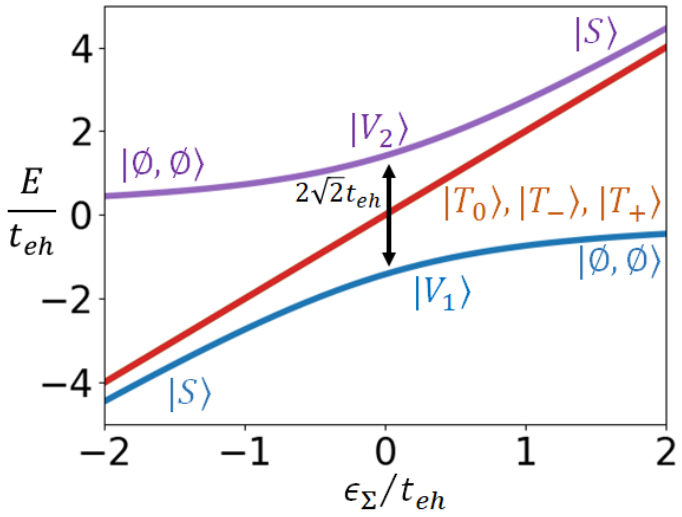

Figure 5.2: Predicted anti-crossing of the double QD energy levels as a function of the chemical potential sum ϵ_Σ. This diagram provides a direct measure of the coherent hopping t_{eh} of a single Cooper pair between the superconductor and the QDs. This anti-crossing will be measured with a microwave resonator which couples to the transition between the system eigenstates $|V_1\rangle$ and $|V_2\rangle$. When $\epsilon_\Sigma \gg t_{eh}$, $|V_2\rangle$ resembles the singlet state $|S\rangle$, and $|V_1\rangle$ the doubly unoccupied state $|\emptyset,\emptyset\rangle$, and these roles are reversed for $\epsilon_\Sigma \ll t_{eh}$. The red straight line covers the three degenerate eigenenergies corresponding to the three triplet states $|T_{0,+,-}\rangle$.

5.2.2 Cavity-enhanced single-spin spontaneous emission

Once the CP is transferred from the superconducting lead to the double QD, its spin entanglement needs to be converted into the entanglement of two photons. This conversion relies on a spin-photon coupling, which we plan to measure in this step. Since the natural spin-photon coupling is weak, we will synthesize a spin-orbit interaction which, with the strong natural charge-photon coupling, leads to a strong synthetic spin-photon coupling. This has been

achieved by using non-collinear ferromagnetic leads [Viennot et al., 2015, Cubaynes et al., 2019]. We now give an intuitive picture of the origin of this synthetic spin-photon coupling. Let us assume for definiteness that the double QD is initially only populated with a spin up electron in the left dot, with a spin quantization axis parallel to the magnetization of the left electrode. The cavity electrical field couples strongly to the electric dipole formed by the two dots, and can hence induce a transition from the left to the right dot, and vice versa. As the electron is transferred to the right dot, it encounters a magnetization which is non collinear to its spin, and hence will precess thus flipping its spin, before being transferred back by the cavity field to the left dot. This process is maximally efficient when the cavity mode is resonant with the energy difference between the two opposite spin states caused be the Zeeman splitting. We will satisfy this resonance condition by tuning the cavity frequency in-situ. The tunability will be possible by interrupting the resonator with a SQUID, thus making the resonator frequency flux dependent. The goal of this task will be to observe the electron spin flip accompanied by a single photon emission in the resonator. The photon will travel through the transmission line towards our detector. The spin-photon coupling can be measured by measuring the increased decay rate γ_s at which the electron spin flips when the resonator is tuned into resonance [Bienfait et al., 2016]. We find $\gamma_s = 4{g_s}^2/\kappa_r$, where g_s is the spin photon coupling rate and κ_r is the resonator energy decay rate. Assuming $g_s = 2\pi\times 1$ MHz [Cubaynes et al., 2019], and $\kappa_r = 2\pi \times 4$ MHz, we find $\gamma_s = 2\pi \times 1$ MHz, which is more than a factor of two greater than the natural dephasing time of the spin transition [Cubaynes et al., 2019]. Hence this accelerated decay should be observable, leading to the observation of a single photon emitted by a single electron spin flip. The nature of the emitted photon will further be investigated using state of the art quantum limited amplifiers.

5.2.3 Measuring the entanglement of the radiation emitted by a single Cooper pair

Using the results of the two previous tasks, we will fabricate a device capable of measuring the spin entanglement of a single CP. Each QD will be coupled to a separate microwave cavity. Starting from the doubly unoccupied state, we will tune the gate voltages to bring the left and right dots into resonance with the superconducting lead. As soon as the CP is transferred, the swap will be interrupted by moving the dots out of resonance with the superconducting lead. By tuning the gate voltages and flux in each cavity accordingly, we will induce the transition between the singlet state and the state with both electrons in spin down. This transition will be

accompanied by the emission of two entangled microwave photons (see Fig. 5.3). The emitted photons can be measured using state of the art quantum limited parametric amplifiers. Each cavity will be connected to its custom made amplifier and by analyzing the correlations between the two measurements, we can recover the full density matrix of the two traveling fields [Eichler et al., 2011, Gasparinetti et al., 2017]. We will then back-out the density matrix of the two electrons prior to their photonic emissions.

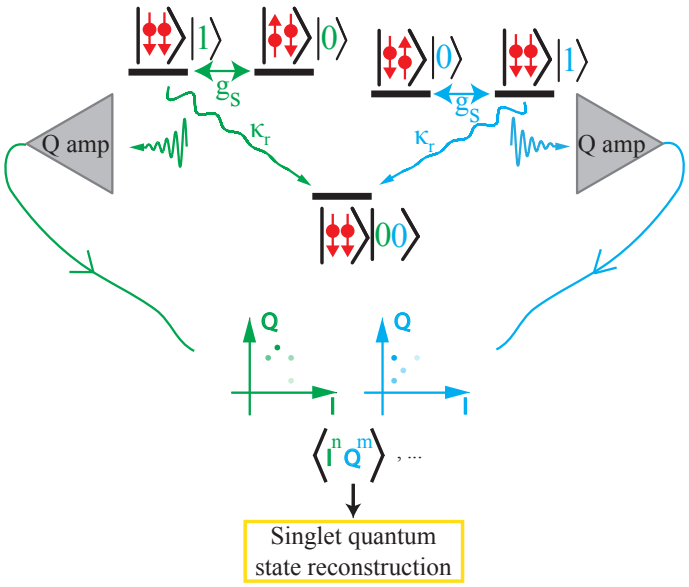

Figure 5.3: Principle of our spin entanglement detector. Two microwave resonators, one coupled to the left dot (green) and another to the right dot (blue), are each tuned into resonance with the left and right spin-flip transition. Starting from a spin singlet state, this results in the emission of an entangled pair of propagating microwave photons. Using state of the art quantum limited amplifiers (triangles) we will detect the (I, Q) quadratures of these fields. By repeating the experiment tens of thousands of times, we will accumulate statistics and calculate correlations (brackets). This will lead to the full state reconstruction of the electronic state prior to the photonic emissions.

5.3 Methods

5.3.1 Fabrication of carbon nanotube devices

This project requires the splitting of a single Cooper pair. For that purpose, we will use a carbon nanotube (CNT) as a 1D conductor, and electrodes will delimit two regions (quantum dots) where electrons can localize. As we have already recently demonstrated [Cubaynes

et al., 2019], we will follow the technique introduced in [Waissman et al., 2013] for the deterministic creation of locally-tunable, ultralow-disorder electron systems in carbon nanotubes suspended over complex electronic circuits. The CNT is mechanically transferred onto the circuit at the very last step of the fabrication process, which is done in two steps.

1. *Circuit chip*: the *circuit* chip will be a Si substrate containing the Nb resonators, the SQUIDS, PdNi electrodes which are non parallel (for non-collinearity of the magnetization, see Fig. 5.4), and back gates. The SQUID Josephson junctions will be fabricated using the standard Dolan bridge technique and double angle evaporation. Aggressive cleaning techniques can be used to get high quality resonators.
2. *CNT growth and stapling*: The CNTs are grown on a separate chip in between micrometric teeth of a comb. This preserves the nanotube during the whole process from any chemical pollution. A micro-manipulator and piezo-electric controller drives the CNT onto the electronic circuit. The integrated CNT can be characterized with conductance measurement (bundles, metallic, semi-conductor, presence of defects). In addition, optical Rayleigh characterization before the transfer can give insight on the semi-conducting gap and chirality of the CNTs. This control on the CNT increases the reproduciblity of the devices. This technique has become very efficient with a dedicated equipment built in-house at the host laboratory and allows a rapid transfer of the CNT under vacuum condition [Cubaynes et al., 2019].

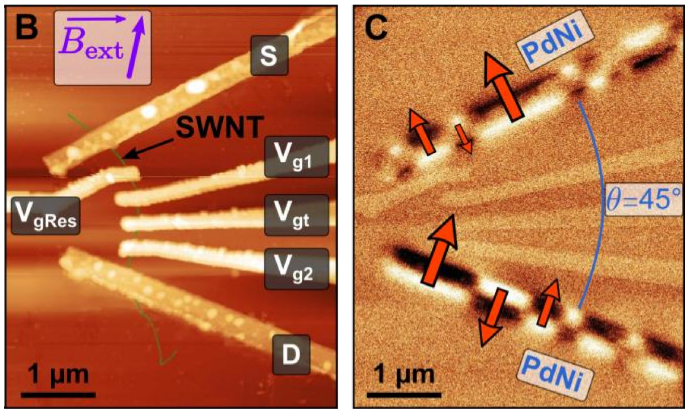

Figure 5.4: Left: atomic force micrograph of a SWCNT (single wall CNT) with three top DC bias gates (Vg1, Vgt, Vg2), and a finger (VgRes) reaching from a superconducting resonator. Right: magnetic force micrograph showing that the source S and drain D electrodes are made out of a ferromagnetic alloy (PdNi). Black and white colors correspond to north and south poles of ferromagnetic domains. Figure from [Viennot et al., 2015]. In this project, I will use this technique to induce spin-photon coupling between a Cooper pair splitter and a cavity.

Chapter 6

Outlook

Can quantum information be encoded over macroscopic timescales ? That is, can an arbitrary unknown quantum state be protected from decoherence for milliseconds, seconds, minutes or even hours ? In theory, nothing prevents quantum error correction protocols from arbitrarily extending the lifetime of quantum information by encoding it across an ever increasing number of degrees of freedom. However, as an experimental physicist, I feel compelled to verify this in the laboratory. The beauty of this quest is that the steps along the way are likely to be at least as intriguing as the end goal. While succeeding would imply lifting one of the major roadblocks towards the emergence of quantum technologies, every order of magnitude improvement in the lifetime promises to unveil mysterious physical phenomena. As we design protocols to correct against errors induced by interactions with local environments, what will we learn about the remaining uncorrected error channels ? I believe that error-corrected quantum bits could be used as low-dark-count probes for correlated noise such as high energy particle impacts caused by cosmic rays or radioactive emissions [Vepsäläinen et al., 2020, Cardani et al., 2020], or even contemplate sensing minuscule traces of decoherence caused by dark matter [Riedel, 2013] or gravity [Diósi, 1987].

Chapter 7

Bibliography

[Aliferis and Preskill, 2008] Aliferis, P. and Preskill, J. (2008). Fault-tolerant quantum computation against biased noise. *Phys. Rev. A*, 78:052331.

[Barends et al., 2014] Barends, R., Kelly, J., Megrant, A., Veitia, A., Sank, D., Jeffrey, E., White, T. C., Mutus, J., Fowler, A. G., Campbell, B., Chen, Y., Chen, Z., Chiaro, B., Dunsworth, A., Neill, C., O'Malley, P., Roushan, P., Vainsencher, A., Wenner, J., Korotkov, A. N., Cleland, A. N., and Martinis, J. M. (2014). Superconducting quantum circuits at the surface code threshold for fault tolerance. *Nature*, 508(7497):500–503.

[Bergeal et al., 2010] Bergeal, N., Schackert, F., Metcalfe, M., Vijay, R., Manucharyan, V. E., Frunzio, L., Prober, D. E., Schoelkopf, R. J., Girvin, S. M., and Devoret, M. H. (2010). Phase-preserving amplification near the quantum limit with a josephson ring modulator. *Nature*, 465:64.

[Bienfait et al., 2016] Bienfait, A., Pla, J. J., Kubo, Y., Zhou, X., Stern, M., Lo, C. C., Weis, C. D., Schenkel, T., Vion, D., Esteve, D., Morton, J. J. L., and Bertet, P. (2016). Controlling spin relaxation with a cavity. *Nature*, 531:74.

[Bravyi and Kitaev, 1998] Bravyi, S. B. and Kitaev, A. Y. (1998). Quantum codes on a lattice with boundary. *arXiv:quant-ph/9811052*.

[Brooks et al., 2013] Brooks, P., Kitaev, A., and Preskill, J. (2013). Protected gates for superconducting qubits. *Phys. Rev. A*, 87:052306.

[Bruno et al., 2015] Bruno, A., de Lange, G., Asaad, S., van der Enden, K. L., Langford, N. K., and DiCarlo, L. (2015). Reducing intrinsic loss in superconducting resonators by surface treatment and deep etching of silicon substrates. *Applied Physics Letters*, 106(18):182601.

[Campagne-Ibarcq et al., 2019] Campagne-Ibarcq, P., Eickbusch, A., Touzard, S., Zalys-Geller, E., Frattini, N. E., Sivak, V. V., Reinhold, P., Puri, S., Shankar, S., Schoelkopf, R. J., Frunzio, L., Mirrahimi, M., and Devoret, M. H. (2019). A stabilized logical quantum bit encoded in grid states of a superconducting cavity. *arXiv:1907.12487*.

[Cao et al., 2005] Cao, J., Wang, Q., and Dai, H. (2005). Electron transport in very clean, as-grown suspended carbon nanotubes. *Nature Materials*, 4:745.

[Cardani et al., 2020] Cardani, L., Valenti, F., Casali, N., Catelani, G., Charpentier, T., Clemenza, M., Colantoni, I., Cruciani, A., Gironi, L., Grünhaupt, L., Gusenkova, D., Henriques, F., Lagoin, M., Martinez, M., Pettinari, G., Rusconi, C., Sander, O., Ustinov, A. V., Weber, M., Wernsdorfer, W., Vignati, M., Pirro, S., and Pop, I. M. (2020). Reducing the impact of radioactivity on quantum circuits in a deep-underground facility.

[Carmichael, 2007] Carmichael, H. J. (2007). *Statistical Methods in Quantum Optics 2*. Springer.

[Carusotto and Ciuti, 2013] Carusotto, I. and Ciuti, C. (2013). Quantum fluids of light. *Reviews of Modern Physics*, 85(1):299–366.

[Childress et al., 2004] Childress, L., Sørensen, A. S., and Lukin, M. D. (2004). Mesoscopic cavity quantum electrodynamics with quantum dots. *Phys. Rev. A*, 69:042302.

[Cohen et al., 2017] Cohen, J., Smith, W. C., Devoret, M. H., and Mirrahimi, M. (2017). Degeneracy-preserving quantum nondemolition measurement of parity-type observables for cat qubits. *Phys. Rev. Lett.*, 119:060503.

[Corcoles et al., 2015] Corcoles, A. D., Magesan, E., Srinivasan, S. J., Cross, A. W., Steffen, M., Gambetta, J. M., and Chow, J. M. (2015). Demonstration of a quantum error detection code using a square lattice of four superconducting qubits. *Nature Communications*, 6:6979–6979.

[Cottet, 2012] Cottet, A. (2012). Microwave spectroscopy of a cooper pair beam splitter. *Phys. Rev. B*, 86:075107.

[Cottet and Kontos, 2010] Cottet, A. and Kontos, T. (2010). Spin quantum bit with ferromagnetic contacts for circuit qed. *Phys. Rev. Lett.*, 105:160502.

[Cubaynes et al., 2019] Cubaynes, T., Delbecq, M. R., Dartiailh, M. C., Assouly, R., Desjardins, M. M., Contamin, L. C., Bruhat, L. E., Leghtas, Z., Mallet, F., Cottet, A., and Kontos, T. (2019). Highly coherent spin states in carbon nanotubes coupled to cavity photons. *npj Quantum Information*, 5(1):47.

[Delbecq et al., 2011] Delbecq, M. R., Schmitt, V., Parmentier, F. D., Roch, N., Viennot, J. J., Feve, G., Huard, B., Mora, C., Cottet, A., and Kontos, T. (2011). Coupling a quantum dot, fermionic leads, and a microwave cavity on a chip. *Physical Review Letters*, 107(25):256804.

[Desjardins et al., 2017] Desjardins, M. M., Viennot, J. J., Dartiailh, M. C., Bruhat, L. E., Delbecq, M. R., Lee, M., Choi, M.-S., Cottet, A., and Kontos, T. (2017). Observation of the frozen charge of a kondo resonance. *Nature*, 545:71.

[Devoret and Schoelkopf, 2013] Devoret, M. H. and Schoelkopf, R. J. (2013). Superconducting circuits for quantum information: An outlook. *Science*, 339:1169.

[Diósi, 1987] Diósi, L. (1987). A universal master equation for the gravitational violation of quantum mechanics. *Physics Letters A*, 120(8):377–381.

[Douçot et al., 2005] Douçot, B., Feigel'man, M. V., Ioffe, L. B., and Ioselevich, A. S. (2005). Protected qubits and chern-simons theories in josephson junction arrays. *Phys. Rev. B*, 71:024505.

[Douçot and Vidal, 2002] Douçot, B. and Vidal, J. (2002). Pairing of cooper pairs in a fully frustrated josephson-junction chain. *Phys. Rev. Lett.*, 88:227005.

[Eichler et al., 2011] Eichler, C., Bozyigit, D., Lang, C., Steffen, L., Fink, J., and Wallraff, A. (2011). Experimental state tomography of itinerant single microwave photons. *Phys. Rev. Lett.*, 106:220503.

[Flurin et al., 2015] Flurin, E., Roch, N., Pillet, J. D., Mallet, F., and Huard, B. (2015). Superconducting quantum node for entanglement and storage of microwave radiation. *Physical Review Letters*, 114(9):090503.

[Fowler et al., 2012] Fowler, A. G., Mariantoni, M., Martinis, J. M., and Cleland, A. N. (2012). Surface codes: Towards practical large-scale quantum computation. *Physical Review A*, 86(3):032324.

[Frattini et al., 2017] Frattini, N. E., Vool, U., Shankar, S., Narla, A., Sliwa, K. M., and Devoret, M. H. (2017). 3-wave mixing josephson dipole element.

[Gao et al., 2018] Gao, Y. Y., Lester, B. J., Zhang, Y., Wang, C., Rosenblum, S., Frunzio, L., Jiang, L., Girvin, S. M., and Schoelkopf, R. J. (2018). Programmable interference between two microwave quantum memories. *Phys. Rev. X*, 8:021073.

[Gasparinetti et al., 2017] Gasparinetti, S., Pechal, M., Besse, J.-C., Mondal, M., Eichler, C., and Wallraff, A. (2017). Correlations and entanglement of microwave photons emitted in a cascade decay. *Phys. Rev. Lett.*, 119:140504.

[Geerlings et al., 2013] Geerlings, K., Leghtas, Z., Pop, I. M., Shankar, S., Frunzio, L., Schoelkopf, R. J., Mirrahimi, M., and Devoret, M. H. (2013). Demonstrating a driven reset protocol for a superconducting qubit. *Phys. Rev. Lett.*, 110:120501.

[Girvin, 2011] Girvin, S. (2011). Quantum information processing with superconducting circuits. *Les Houches Session XCVI, Quantum machines*, pages 113–239.

[Gladchenko et al., 2008] Gladchenko, S., Olaya, D., Dupont-Ferrier, E., Douçot, B., Ioffe, L. B., and Gershenson, M. E. (2008). Superconducting nanocircuits for topologically protected qubits. *Nature Physics*, 5:48.

[Gottesman et al., 2001] Gottesman, D., Kitaev, A., and Preskill, J. (2001). Encoding a qubit in an oscillator. *Phys. Rev. A*, 64:012310.

[Grimm et al., 2019] Grimm, A., Frattini, N. E., Puri, S., Mundhada, S. O., Touzard, S., Mirrahimi, M., Girvin, S. M., Shankar, S., and Devoret, M. H. (2019). The kerr-cat qubit: Stabilization, readout, and gates. *arXiv:1907.12131*.

[Groszkowski et al., 2018] Groszkowski, P., Paolo, A. D., Grimsmo, A. L., Blais, A., Schuster, D. I., Houck, A. A., and Koch, J. (2018). Coherence properties of the 0-^{1} qubit. *New Journal of Physics*, 20(4):043053.

[Grünhaupt et al., 2018] Grünhaupt, L., Maleeva, N., Skacel, S. T., Calvo, M., Levy-Bertrand, F., Ustinov, A. V., Rotzinger, H., Monfardini, A., Catelani, G., and Pop, I. M. (2018). Loss mechanisms and quasiparticle dynamics in superconducting microwave resonators made of thin-film granular aluminum. *Phys. Rev. Lett.*, 121:117001.

[Guillaud and Mirrahimi, 2019] Guillaud, J. and Mirrahimi, M. (2019). Repetition cat qubits for fault-tolerant quantum computation. *Phys. Rev. X*, 9:041053.

[Haikka et al., 2017] Haikka, P., Kubo, Y., Bienfait, A., Bertet, P., and Mølmer, K. (2017). Proposal for detecting a single electron spin in a microwave resonator. *Phys. Rev. A*, 95:022306.

[Haroche and Raimond, 2006] Haroche, S. and Raimond, J. (2006). *Exploring the Quantum: Atoms, Cavities and Photons.* Oxford University Press.

[Hatridge et al., 2013] Hatridge, M., Shankar, S., Mirrahimi, M., Schackert, F., Geerlings, K., Brecht, T., Sliwa, K. M., Abdo, B., Frunzio, L., Girvin, S. M., Schoelkopf, R. J., and Devoret, M. H. (2013). Quantum back-action of an individual variable-strength measurement. *Science*, 339(6116):178.

[Hays et al., 2018] Hays, M., de Lange, G., Serniak, K., van Woerkom, D. J., Bouman, D., Krogstrup, P., Nygård, J., Geresdi, A., and Devoret, M. H. (2018). Direct microwave measurement of andreev-bound-state dynamics in a semiconductor-nanowire josephson junction. *Phys. Rev. Lett.*, 121:047001.

[Ioffe and Feigel'man, 2002] Ioffe, L. B. and Feigel'man, M. V. (2002). Possible realization of an ideal quantum computer in josephson junction array. *Phys. Rev. B*, 66:224503.

[Kamal et al., 2009] Kamal, A., Marblestone, A., and Devoret, M. H. (2009). Signal-to-pump back action and self- oscillation in double-pump josephson parametric amplifier. *Phys. Rev. B.*, 79(184301).

[Kelly et al., 2015] Kelly, J., Barends, R., Fowler, A. G., Megrant, A., Jeffrey, E., White, T. C., Sank, D., Mutus, J. Y., Campbell, B., Chen, Y., Chen, Z., Chiaro, B., Dunsworth, A., Hoi, I. . C., Neill, C., O'Malley, P. J. J., Quintana, C., Roushan, P., Vainsencher, A., Wenner, J., Cleland, A. N., and Martinis, J. M. (2015). State preservation by repetitive error detection in a superconducting quantum circuit. *Nature*, 519(7541):66–69.

[Kirchmair et al., 2013a] Kirchmair, G., Vlastakis, B., Leghtas, Z., Nigg, S. E., Paik, H., Ginossar, E., Mirrahimi, M., Frunzio, L., Girvin, S. M., and Schoelkopf, R. J. (2013a). Observation of quantum state collapse and revival due to the single-photon kerr effect. *Nature*, 495:205.

[Kirchmair et al., 2013b] Kirchmair, G., Vlastakis, B., Leghtas, Z., Nigg, S. E., Paik, H., Ginossar, E., Mirrahimi, M., Frupzio, L., Girvin, S. M., and Schoelkopf, R. J. (2013b). Obser-

vation of quantum state collapse and revival due to the single-photon kerr effect. *Nature*, 495(7440):205–209.

[Kitaev, 2006] Kitaev, A. (2006). Protected qubit based on a superconducting current mirror. *arXiv:cond-mat/0609441*.

[Kitaev, 2003] Kitaev, A. Y. (2003). Fault-tolerant quantum computation by anyons. *Annals of Physics*, 303(1):2–30.

[Kouwenhoven et al., 2001] Kouwenhoven, L. P., Austing, D. G., and Tarucha, S. (2001). Few-electron quantum dots. *Reports on Progress in Physics*, 64(6):701.

[Kreikebaum et al., 2016] Kreikebaum, J. M., Dove, A., Livingston, W., Kim, E., and Siddiqi, I. (2016). Optimization of infrared and magnetic shielding of superconducting tin and al coplanar microwave resonators. *Superconductor Science and Technology*, 29(10):104002.

[Laird et al., 2015] Laird, E. A., Kuemmeth, F., Steele, G. A., Grove-Rasmussen, K., Nygård, J., Flensberg, K., and Kouwenhoven, L. P. (2015). Quantum transport in carbon nanotubes. *Rev. Mod. Phys.*, 87:703–764.

[Leghtas et al., 2013a] Leghtas, Z., Kirchmair, G., Vlastakis, B., Schoelkopf, R. J., Devoret, M. H., and Mirrahimi, M. (2013a). Hardware-efficient autonomous quantum memory protection. *Physical Review Letters*, 111(12):120501.

[Leghtas et al., 2015] Leghtas, Z., Touzard, S., Pop, I. M., Kou, A., Vlastakis, B., Petrenko, A., Sliwa, K. M., Narla, A., Shankar, S., Hatridge, M. J., Reagor, M., Frunzio, L., Schoelkopf, R. J., Mirrahimi, M., and Devoret, M. H. (2015). Confining the state of light to a quantum manifold by engineered two-photon loss. *Science*, 347(6224):853–857.

[Leghtas et al., 2013b] Leghtas, Z., Vool, U., Shankar, S., Hatridge, M., Girvin, S. M., Devoret, M. H., and Mirrahimi, M. (2013b). Stabilizing a bell state of two superconducting qubits by dissipation engineering. *Physical Review A*, 88(2):023849.

[Lescanne et al., 2019] Lescanne, R., Verney, L., Ficheux, Q., Devoret, M. H., Huard, B., Mirrahimi, M., and Leghtas, Z. (2019). Escape of a driven quantum josephson circuit into unconfined states. *Phys. Rev. Applied*, 11:014030.

[Lescanne et al., 2020] Lescanne, R., Villiers, M., Peronnin, T., Sarlette, A., Delbecq, M., Huard, B., Kontos, T., Mirrahimi, M., and Leghtas, Z. (2020). Exponential suppression of bit-flips in a qubit encoded in an oscillator. *Nature Physics*, 16(5):509–513.

[Lin et al., 2018] Lin, Y.-H., Nguyen, L. B., Grabon, N., San Miguel, J., Pankratova, N., and Manucharyan, V. E. (2018). Demonstration of protection of a superconducting qubit from energy decay. *Phys. Rev. Lett.*, 120:150503.

[Maleeva et al., 2018] Maleeva, N., Grünhaupt, L., Klein, T., Levy-Bertrand, F., Dupre, O., Calvo, M., Valenti, F., Winkel, P., Friedrich, F., Wernsdorfer, W., Ustinov, A. V., Rotzinger, H., Monfardini, A., Fistul, M. V., and Pop, I. M. (2018). Circuit quantum electrodynamics of granular aluminum resonators. *Nature Communications*, 9(1):3889.

[Manucharyan, 2012] Manucharyan, V. E. (2012). *Superinductance*. PhD thesis.

[Manucharyan et al., 2009] Manucharyan, V. E., Koch, J., Glazman, L. I., and Devoret, M. H. (2009). Fluxonium: Single cooper-pair circuit free of charge offsets. *Science*, 326(5949):113.

[Masluk et al., 2012] Masluk, N. A., Pop, I. M., Kamal, A., Minev, Z. K., and Devoret, M. H. (2012). Microwave characterization of josephson junction arrays: Implementing a low loss superinductance. *Phys. Rev. Lett.*, 109:137002.

[Mi et al., 2018] Mi, X., Benito, M., Putz, S., Zajac, D. M., Taylor, J. M., Burkard, G., and Petta, J. R. (2018). A coherent spin-photon interface in silicon. *Nature*, 555:599.

[Mirrahimi et al., 2014] Mirrahimi, M., Leghtas, Z., Albert, V. V., Touzard, S., Schoelkopf, R. J., Jiang, L., and Devoret, M. H. (2014). Dynamically protected cat-qubits: a new paradigm for universal quantum computation. *New J. Phys.*, 16(4):045014.

[Nielsen and Chuang, 2000] Nielsen, M. and Chuang, I. (2000). *Quantum Computation and Quantum Information*. Cambridge University Press.

[Nigg et al., 2012] Nigg, S. E., Paik, H., Vlastakis, B., Kirchmair, G., Shankar, S., Frunzio, L., Devoret, M. H., Schoelkopf, R. J., and Girvin, S. M. (2012). Black-box superconducting circuit quantization. *Phys. Rev. Lett.*, 108:240502.

[Ofek et al., 2016] Ofek, N., Petrenko, A., Heeres, R., Reinhold, P., Leghtas, Z., Vlastakis, B., Liu, Y., Frunzio, L., Girvin, S. M., Jiang, L., Mirrahimi, M., Devoret, M. H., and Schoelkopf, R. J. (2016). Extending the lifetime of a quantum bit with error correction in superconducting circuits. *Nature*, 536:441.

[Otterbach et al., 2017] Otterbach, J. S., Manenti, R., Alidoust, N., Bestwick, A., Block, M., Bloom, B., Caldwell, S., Didier, N., Fried, E. S., Hong, S., Karalekas, P., Osborn, C. B., Papageorge, A., Peterson, E. C., Prawiroatmodjo, G., Rubin, N., Ryan, C. A., Scarabelli, D.,

Scheer, M., Sete, E. A., Sivarajah, P., Smith, R. S., Staley, A., Tezak, N., Zeng, W. J., Hudson, A., Johnson, B. R., Reagor, M., da Silva, M. P., and Rigetti, C. (2017). Unsupervised machine learning on a hybrid quantum computer.

[Pechenezhskiy et al., 2019] Pechenezhskiy, I. V., Mencia, R. A., Nguyen, L. B., Lin, Y.-H., and Manucharyan, V. E. (2019). Quantum dynamics of quasicharge in an ultrahigh-impedance superconducting circuit.

[Peruzzo et al., 2020] Peruzzo, M., Trioni, A., Hassani, F., Zemlicka, M., and Fink, J. M. (2020). Surpassing the resistance quantum with a geometric superinductor. *arXiv:2007.01644*.

[Pop et al., 2014] Pop, I. M., Geerlings, K., Catelani, G., Schoelkopf, R. J., Glazman, L. I., and Devoret, M. H. (2014). Coherent suppression of electromagnetic dissipation due to superconducting quasiparticles. *Nature*, 508:369.

[Puri et al., 2019] Puri, S., St-Jean, L., Gross, J. A., Grimm, A., Frattini, N. E., Iyer, P. S., Krishna, A., Touzard, S., Jiang, L., Blais, A., Flammia, S. T., and Girvin, S. M. (2019). Bias-preserving gates with stabilized cat qubits. *arXiv:1905.00450*.

[Reagor et al., 2016] Reagor, M., Pfaff, W., Axline, C., Heeres, R. W., Ofek, N., Sliwa, K., Holland, E., Wang, C., Blumoff, J., Chou, K., Hatridge, M. J., Frunzio, L., Devoret, M. H., Jiang, L., and Schoelkopf, R. J. (2016). Quantum memory with millisecond coherence in circuit qed. *Phys. Rev. B*, 94:014506.

[Recher et al., 2001] Recher, P., Sukhorukov, E. V., and Loss, D. (2001). Andreev tunneling, coulomb blockade, and resonant transport of nonlocal spin-entangled electrons. *Phys. Rev. B*, 63:165314.

[Reed et al., 2012] Reed, M., DiCarlo, L., Nigg, S., Sun, L., Frunzio, L., Girvin, S., and Schoelkopf, R. (2012). Realization of three-qubit quantum error correction with superconducting circuits. *Nature*, 482:382–385.

[Riedel, 2013] Riedel, C. J. (2013). Direct detection of classically undetectable dark matter through quantum decoherence. *Phys. Rev. D*, 88:116005.

[Riste et al., 2015] Riste, D., Poletto, S., Huang, M. . Z., Bruno, A., Vesterinen, V., Saira, O. . P., and DiCarlo, L. (2015). Detecting bit-flip errors in a logical qubit using stabilizer measurements. *Nature communications*, 6:6983–6983.

[Samkharadze et al., 2018] Samkharadze, N., Zheng, G., Kalhor, N., Brousse, D., Sammak, A., Mendes, U. C., Blais, A., Scappucci, G., and Vandersypen, L. M. K. (2018). Strong spin-photon coupling in silicon. *Science*.

[Sank et al., 2016] Sank, D., Chen, Z., Khezri, M., Kelly, J., Barends, R., Campbell, B., Chen, Y., Chiaro, B., Dunsworth, A., Fowler, A., Jeffrey, E., Lucero, E., Megrant, A., Mutus, J., Neeley, M., Neill, C., O'Malley, P. J. J., Quintana, C., Roushan, P., Vainsencher, A., White, T., Wenner, J., Korotkov, A. N., and Martinis, J. M. (2016). Measurement-induced state transitions in a superconducting qubit: Beyond the rotating wave approximation. *Phys. Rev. Lett.*, 117:190503.

[Sarlette et al., 2012] Sarlette, A., Leghtas, Z., Brune, M., Raimond, J. M., and Rouchon, P. (2012). Stabilization of nonclassical states of one- and two-mode radiation fields by reservoir engineering. *Physical Review A*, 86(1):012114.

[Schackert et al., 2013] Schackert, F., Roy, A., Hatridge, M., Devoret, M. H., and Stone, A. D. (2013). Three-wave mixing with three incoming waves: Signal-idler coherent attenuation and gain enhancement in a parametric amplifier. *Physical Review Letters*, 111(7):073903.

[Schuster et al., 2007] Schuster, D., Houck, A., Schreier, J., Wallraff, A., Gambetta, J., Blais, A., Frunzio, L., Majer, J., Johnson, B., Devoret, M., Girvin, S., and Schoelkopf, R. J. (2007). Resolving photon number states in a superconducting circuit. *Nature*, 445:515–518.

[Serniak et al., 2018] Serniak, K., Hays, M., de Lange, G., Diamond, S., Shankar, S., Burkhart, L. D., Frunzio, L., Houzet, M., and Devoret, M. H. (2018). Hot non-equilibrium quasiparticles in transmon qubits.

[Shankar et al., 2013] Shankar, S., Hatridge, M., Leghtas, Z., Sliwa, K. M., Narla, A., Vool, U., Girvin, S. M., Frunzio, L., Mirrahimi, M., and Devoret, M. H. (2013). Autonomously stabilized entanglement between two superconducting quantum bits. *Nature*, 504(7480):419–+.

[Shearrow et al., 2018] Shearrow, A., Koolstra, G., Whiteley, S. J., Earnest, N., Barry, P. S., Heremans, F. J., Awschalom, D. D., Shirokoff, E., and Schuster, D. I. (2018). Atomic layer deposition of titanium nitride for quantum circuits.

[Shor, 1995] Shor, P. (1995). Scheme for reducing decoherence in quantum memory. *Phys. Rev. A*, 52:2493–2496.

[Shor, 1996] Shor, W. P. (1996). Fault-tolerant quantum computation. *37th Symposium on Foundations of Computing, IEEE Computer Society Press*, pages 56–65. arXiv:quant-ph/9605011.

[Smith, 2020] Smith, W. C. (2020). *Design of protected superconducting qubits*. PhD thesis, Yale University.

[Smith et al., 2020a] Smith, W. C., Kou, A., Xiao, X., Vool, U., and Devoret, M. H. (2020a). Superconducting circuit protected by two-cooper-pair tunneling. *npj Quantum Information*, 6(1):8.

[Smith et al., 2020b] Smith, W. C., Villiers, M., Marquet, A., Palomo, J., Delbecq, M. R., Kontos, T., Campagne-Ibarcq, P., Douçot, B., and Leghtas, Z. (2020b). Magnifying quantum phase fluctuations with cooper-pair pairing. *arXiv:2010.15488*.

[Steane, 1996] Steane, A. (1996). Error correcting codes in quantum theory. *Phys. Rev. Lett*, 77(5).

[Sun et al., 2014] Sun, L., Petrenko, A., Leghtas, Z., Vlastakis, B., Kirchmair, G., Sliwa, K. M., Narla, A., Hatridge, M., Shankar, S., Blumoff, J., Frunzio, L., Mirrahimi, M., Devoret, M. H., and Schoelkopf, R. J. (2014). Tracking photon jumps with repeated quantum non-demolition parity measurements. *Nature*, 511(7510):444–+.

[Teufel et al., 2011] Teufel, J. D., Donner, T., Li, D., Harlow, J. W., Allman, M. S., Cicak, K., Sirois, A. J., Whittaker, J. D., Lehnert, K. W., and Simmonds, R. W. (2011). Sideband cooling of micromechanical motion to the quantum ground state. *Nature*, 475(7356):359–363.

[Tosi et al., 2014] Tosi, G., Mohiyaddin, F. A., Huebl, H., and Morello, A. (2014). Circuit-quantum electrodynamics with direct magnetic coupling to single-atom spin qubits in isotopically enriched 28si. *AIP Advances*, 4(8):087122.

[Tosi et al., 2019] Tosi, L., Metzger, C., Goffman, M. F., Urbina, C., Pothier, H., Park, S., Yeyati, A. L., Nygård, J., and Krogstrup, P. (2019). Spin-orbit splitting of andreev states revealed by microwave spectroscopy. *Phys. Rev. X*, 9:011010.

[Touzard et al., 2018a] Touzard, S., Grimm, A., Leghtas, Z., Mundhada, S. O., Reinhold, P., Axline, C., Reagor, M., Chou, K., Blumoff, J., Sliwa, K. M., Shankar, S., Frunzio, L., Schoelkopf, R. J., Mirrahimi, M., and Devoret, M. H. (2018a). Coherent oscillations inside a quantum manifold stabilized by dissipation. *Phys. Rev. X*, 8:021005.

[Touzard et al., 2018b] Touzard, S., Grimm, A., Leghtas, Z., Mundhada, S. O., Reinhold, P., Axline, C., Reagor, M., Chou, K., Blumoff, J., Sliwa, K. M., Shankar, S., Frunzio, L., Schoelkopf, R. J., Mirrahimi, M., and Devoret, M. H. (2018b). Coherent oscillations inside a quantum manifold stabilized by dissipation. *Phys. Rev. X*, 8:021005.

[Touzard et al., 2019] Touzard, S., Kou, A., Frattini, N. E., Sivak, V. V., Puri, S., Grimm, A., Frunzio, L., Shankar, S., and Devoret, M. H. (2019). Gated conditional displacement readout of superconducting qubits. *Phys. Rev. Lett.*, 122:080502.

[Tuckett et al., 2018] Tuckett, D. K., Bartlett, S. D., and Flammia, S. T. (2018). Ultrahigh error threshold for surface codes with biased noise. *Phys. Rev. Lett.*, 120:050505.

[Tuckett et al., 2019a] Tuckett, D. K., Bartlett, S. D., Flammia, S. T., and Brown, B. J. (2019a). Fault-tolerant thresholds for the surface code in excess of 5% under biased noise. *arXiv:1907.02554*.

[Tuckett et al., 2019b] Tuckett, D. K., Darmawan, A. S., Chubb, C. T., Bravyi, S., Bartlett, S. D., and Flammia, S. T. (2019b). Tailoring surface codes for highly biased noise. *Physical Review X*, 9(4).

[Vepsäläinen et al., 2020] Vepsäläinen, A., Karamlou, A. H., Orrell, J. L., Dogra, A. S., Loer, B., Vasconcelos, F., Kim, D. K., Melville, A. J., Niedzielski, B. M., Yoder, J. L., Gustavsson, S., Formaggio, J. A., VanDevender, B. A., and Oliver, W. D. (2020). Impact of ionizing radiation on superconducting qubit coherence.

[Verney et al., 2019] Verney, L., Lescanne, R., Devoret, M. H., Leghtas, Z., and Mirrahimi, M. (2019). Structural instability of driven josephson circuits prevented by an inductive shunt. *Phys. Rev. Applied*, 11:024003.

[Viennot et al., 2015] Viennot, J. J., Dartiailh, M. C., Cottet, A., and Kontos, T. (2015). Coherent coupling of a single spin to microwave cavity photons. *Science*, 349(6246):408.

[Vlastakis et al., 2013] Vlastakis, B., Kirchmair, G., Leghtas, Z., Nigg, S. E., Frunzio, L., Girvin, S. M., Mirrahimi, M., Devoret, M. H., and Schoelkopf, R. J. (2013). Deterministically encoding quantum information using 100-photon schrodinger cat states. *Science*, 342(6158):607–610.

[Vrajitoarea et al., 2019] Vrajitoarea, A., Huang, Z., Groszkowski, P., Koch, J., and Houck, A. A. (2019). Quantum control of an oscillator using a stimulated josephson nonlinearity. *Nature Physics*.

[Waissman et al., 2013] Waissman, J., Honig, M., Pecker, S., Benyamini, A., Hamo, A., and Ilani, S. (2013). Realization of pristine and locally tunable one-dimensional electron systems in carbon nanotubes. *Nature Nanotechnology*, 8:569.

[Wang et al., 2015] Wang, C., Axline, C., Gao, Y. Y., Brecht, T., Chu, Y., Frunzio, L., Devoret, M. H., and Schoelkopf, R. J. (2015). Surface participation and dielectric loss in superconducting qubits. *Appl. Phys. Lett.*, 107(16):162601.

[Wang et al., 2014] Wang, C., Gao, Y. Y., Pop, I. M., Vool, U., Axline, C., Brecht, T., Heeres, R. W., Frunzio, L., Devoret, M. H., Catelani, G., Glazman, L. I., and Schoelkopf, R. J. (2014). Measurement and control of quasiparticle dynamics in a superconducting qubit. *Nature Communications*, 5(1).

[Webster et al., 2015] Webster, P., Bartlett, S. D., and Poulin, D. (2015). Reducing the overhead for quantum computation when noise is biased. *Phys. Rev. A*, 92:062309.